Proc. NIPR Symp. Antarct. Meteorites, 4, 263–306, 1991

NEW ENCLAVES IN THE VACA MUERTA MESOSIDERITE: PETROGENESIS AND COMPARISON WITH HED METEORITES

Makoto KIMURA[1], Yukio IKEDA[1], Mitsuru EBIHARA[2] and Martin PRINZ[3]

[1]*Department of Earth Sciences, Faculty of Science, Ibaraki University, 1–1, Bunkyo 2-chome, Mito 310*
[2]*Department of Chemistry, Faculty of Science, Tokyo Metropolitan University, 1, Minami-Osawa 1-chome, Hachioji-shi, Tokyo 192–03*
[3]*American Museum of Natural History, Central Park West at 79th Street, New York, NY 10024–5192, U. S. A.*

Abstract: Thirty-eight new enclaves from the Vaca Muerta mesosiderite have been studied, and detailed SEM-petrography was carried out on fourteen of them. Three are coarse-grained gabbroic ilmenite-free enclaves consisting mainly of pigeonite (En_{56-49}) and plagioclase, seven are fine- to medium-grained ilmenite-bearing enclaves (En_{49-36}) with ophitic to granular texture, and four are breccias. The most important breccias are diogenitic monomict breccias (En_{74-65}) and an olivine-orthopyroxenite monomict breccia (Fo_{73-71}). Reduction-induced orthopyroxene commonly surrounds pigeonite grains in the ilmenite-free enclaves, and occurs rarely in the marginal parts of the ilmenite-bearing enclaves. Whitlockite forms from augite lamellae as a result of reduction, and the ilmenite-free enclaves have been enriched in P_2O_5. Reduction of the ilmenite-free enclaves occurred in the parent body before mixing with Fe-Ni metal on the mesosiderite parent body. In the ilmenite-bearing enclaves reduction occurred on the mesosiderite parent body after Fe-Ni metal was mixed in. Thus, two stages of subsolidus reduction occurred in enclaves. Ilmenite and rutile occur in the ilmenite-bearing and diogenitic enclaves, and various subsolidus reaction textures of chromite, ilmenite, rutile and probably preexisting pseudobrookite are found. Al_2O_3-depleted chromite formed through the decomposition of Cr_2O_3-bearing ilmenite and pseudobrookite. Zircon and baddeleyite were also found in the ilmenite-bearing enclaves, and the latter is the first occurrence reported in mesosiderites. The ilmenite-bearing enclaves always contain baddeleyite, whereas ZrO_2-bearing phases are hardly ever found in HED meteorites. The bulk compositions of the enclaves were analyzed, and found to be more SiO_2-enriched than the HED meteorites. Highly SiO_2-enriched ilmenite-bearing enclaves are especially common, and follow the Nuevo Laredo trend of the eucrites, whereas the other ilmenite-bearing enclaves follow the Stannern trend. The highly SiO_2-enriched enclaves probably formed by fractional crystallization, whereas the other ilmenite-bearing enclaves formed through partial melting. The existence of the highly SiO_2-enriched enclaves may partly explain the SiO_2-rich nature of mesosiderites, in addition to the *in situ* reduction process. Our observations suggest that the parent body and the parental magmas of the enclaves in the mesosiderites were initially different from those of the HED meteorites.

1. Introduction

Mesosiderites are mixtures of Fe-Ni metal and silicates, and the silicates are similar in mineralogy and chemical composition to those in the HED meteorites. However, most of the mesosiderites suffered severe shock and thermal metamorphism (POWELL, 1971; FLORAN, 1978; DELANEY *et al.*, 1981). In addition, mesosiderites are unusally enriched in phosphates and silica minerals (POWELL, 1971; NEHRU *et al.*, 1978, 1980a). These enrichments have been interpreted to be the result of *in situ* reduction, and not by igneous fractionation (HARLOW *et al.*, 1982; AGOSTO *et al.*, 1980; RUBIN and JERDE, 1987; MITTLEFEHLDT *et al.*, 1979). These similarities and differences between mesosiderites and the HED meteorites have caused some controversy with regard to the origin of the mesosiderites. RUBIN and JERDE (1987) prefer the idea that mesosiderite enclaves came from the same parent body as the HED meteorites, whereas MITTLEFEHLDT (1990) and IKEDA *et al.* (1990) argue that they came from different parent bodies, emphasizing the differences between them. Thus, some of the more intriguing problems with regard to mesosiderites may be summarized as follows; (1) Do the crystallization and subsolidus histories of the mesosiderite enclaves occur under the same conditions as the HED magmas?, (2) How do we explain the abundant silica minerals and phosphates in the mesosiderites?, and (3) Do mesosiderite enclaves come from the same parent body as the HED meteorites?

Since the fine-grained silicate fractions of the mesosiderites suffered metamorphism, the best samples to clarify the above problems are the large silicate inclusions in mesosiderites. These enclaves may have experienced little or no metamorphism because of their large (often >2 cm) size. They were first studied by MCCALL (1966), and have been called pebbles, clasts or enclaves. Here we call them enclaves after MCCALL (1966), DELANEY *et al.* (1982) or IKEDA *et al.* (1990). The Vaca Muerta mesosiderite, the host of the enclaves studied here, shows the lowest degree of metamorphism (POWELL, 1971), suggesting that the enclaves have not suffered severe metamorphism.

Recently RUBIN and JERDE (1987, 1988), MITTLEFEHLDT (1990), and IKEDA *et al.* (1990) have systematically studied enclaves. Here, we present the results of a new mineralogic and petrologic study of 38 more enclaves, with major and trace element data. We discuss the stages of reduction, the crystallization histories of the enclave magmas, the SiO_2-enriched nature of the enclaves, and compare the enclaves with HED meteorites.

2. Samples and Analytical Procedures

The 38 new enclaves studied come from the American Museum of Natural History meteorite collection (Table 1), and detailed SEM-petrography was carried out on fourteen of the enclaves selected from them.

The chemical compositions of the constituent minerals were measured with a JEOL 733 type electron-probe microanalyzer (EPMA). The accelerating voltage was 15 kV. The Bence-Albee correction method was used for the analysis of the silicates and common oxides, and the ZAF method was used for the ZrO_2-bearing phases, phosphates and metals. The counting times for peak and beam current were

Table 1. Summary of petrography and mineralogy of 38 enclaves.

Enclave	Group	SEM	Texture	Grain size	Replacement	Ave Pig	Ave Opx	Ave An	Ilmenite
4657	I-b	+	op	m-f		35.7		89.3	+
4661	I-b		gb	m		36.1		89.6	+
4671	I-b	+	op	m		36.7		89.2	+
4673	I-b		gr	m	+	40.7		90.9	+
4676	I-b		c-m	c-m	+	38.0		90.0	+
4677	I-b	+	op	m-f		44.2		89.9	+
4678	I-b	+	gr-gb	c-m	+	39.1	55.1	89.7	+
4679	I-b	+	op	c-f		37.5		90.7	+
4681	I-b		gb	m		40.6		90.8	+
4683	I-b	+	gb-do	c		40.4		89.1	+
4684	I-b		gb	c-m	+	43.3	43.3	58.4	+
4686	I-b		gb-gr	c-m	+	42.9	54.6	91.2	+
4690	I-b		op	c-m		38.5		91.0	+
4692	I-b		gb-gr	m	+	44.3	52.6	89.6	+
4695	I-b	+	op	m	+	40.1	52.6	90.4	+
4654	I-f		gb	c	++	52.3		92.8	
4655	I-f		gb-gr	c	++	54.0	56.3	94.2	
4658	I-f		gb	c	++	55.1	58.5	95.5	
4663	I-f		gb	c-m	++	50.3		93.1	
4664	I-f		gb	c	++	55.7		94.0	
4667	I-f		gb	c	++	51.3	55.3	93.7	
4668	I-f		gb	c	++	53.4	60.6	94.1	
4669	I-f	+	gb-gr	c-m		48.9		93.1	
4672	I-f	+	gb	c	++	56.0	58.5	94.9	
4674	I-f	+	gb	c	++	54.4	60.5	93.3	
4682	I-f		gb	c-m	++	49.9		92.5	
4685	I-f		gb-gr	c	+	50.5	53.9	92.9	
4688	I-f		gb	c	++	50.7	53.9	92.2	
4694	I-f		gb-gr	c	+	49.4	55.1	92.7	
4697	I-f		gb	c	++	54.7	57.5	94.5	
4656	B		breccia	f	+	63.0		91.5	+
4659	B	+	breccia				71.2		+
4660	B		breccia	f-m		48.5		90.2	+
4665	B		breccia	f		43.5		92.1	+
4666	B		breccia	f-m		51.8		90.8	+
4670	B	+	breccia	m-f			74.4	94.4	
4687	B	+	breccia	f-m		47.1	53.1	92.3	+
4689	B	+	breccia	f			65.2	89.6	+

SEM petrography was carried out on 14 enclaves (SEM).
Group I-b: ilm-bearing, I-f: ilm-free, B: breccia.
Texture gb: gabbroic, gr: granular, op: ophitic, do: doleritic.
Grain size c: coarse, m: medium, f: fine.
Replacement: replacement of pigeonite by orthopyroxene, ++: remarkable, +: weak.
Ave Pig/Opx: average enstatite mole % of pigeonite and/or orthopyroxene.
Ave An: average anorthite mole % of plagioclase.

usually 20 and 3 to 10 nA, respectively, whereas those for Ce_2O_3, Y_2O_3 and Nd_2O_3 was 60 s and 20 nA, respectively. A special X-ray peak deconvolution program was applied to correct for X-ray overlaps between TiO_2 and V_2O_3 of chromites. The

HfO_2 contents of the ZrO_2-bearing phases were analyzed using a pure HfO_2 standard and a counting time of 40 s for peak and background. The standard deviation (1 sigma) of HfO_2 was 0.15 for zircon containing 0.78 wt% HfO_2. The detection limits (3 sigma) are 0.026 wt% for Ce_2O_3, 0.026 for Nd_2O_3, 0.014 for Y_2O_3, and 0.081 for HfO_2.

Modal analyses were made with the same methods as IKEDA *et al.* (1990), by a step-scanning method using the EPMA. We measured the counts of Si, Ca, Fe, S, Cr and Ti to identify each phase. The point count number for each sample was 2500, and the covered area about 0.5–1.0 cm^2. Then, we calculated the volume percents of low-Ca pyroxene, high-Ca pyroxene, olivine, silica-mineral, phosphate, chromite, ilmenite, rutile, troilite, and Fe-Ni metal.

Glass beads of the enclaves poor in opaque minerals were prepared by heating about 200 mg powdered sample with Pt wires at 1350°C for 15 min. No relict minerals and newly crystallized phases were observed in the glasses. The glasses are homogeneous in composition, even near Pt wires, and the concentrations of Fe in Pt wires were below detection. Major elemental compositions, including P_2O_5, were determined with a broad beam (40 microns in diameter) of the EPMA. The bulk composition of each enclave was calculated from the average composition of about ten point analyses. We also measured the bulk compositions of some enclaves in the Vaca Muerta and Mt. Padbury mesosiderites previously studied by IKEDA *et al.* (1990). The bulk composition of an olivine-orthopyroxenitic enclave 4670 and a troilite-rich enclave 4677, partly brecciated, was calculated from modal and mineralogical data. The bulk compositions of the diogenitic enclave and orthopyroxene-rich clast were calculated by using the average composition of the orthopyroxene, since the other phases have very low abundances.

The concentrations of trace elements were nondestructively analyzed by instrumental neutron activation analysis (INAA), using powdered samples of about 300 mg. About 30 mg of each sample was first irradiated for 100 s in a pneumatic tube (neutron flux 1.5×10^{12}n/$cm^2\cdot$s) for the determination of V and Na. Samples were then irradiated for 6 hours at the same flux for the determination of Sc, Co, Ni, Se, Hf, Ir, Au and some REE (La, Ce, Sm, Eu, Yb and Lu). Neutron irradiations were carried out at the Institute of Atomic Energy, Rikkyo University. The analytical procedures are essentially the same as described in IKEDA *et al.* (1990). The Na contents determined by INAA were the same as those by the EPMA.

3. Petrography

We classified the 38 enclaves into three groups—ilmenite-bearing (ilm-bearing, hereafter), ilmenite-free (ilm-free) and breccia (Table 1)—on the basis of their textures and/or mineralogy (IKEDA *et al.*, 1990). Ilm-bearing enclaves are basaltic to gabbroic, and mineralogically characterized by FeO-rich pyroxene and TiO_2-oxides (ilmenite and rutile), whereas ilm-free enclaves are gabbroic and include FeO-poor pyroxene and no TiO_2-oxides. RUBIN and JERDE (1988) and MITTLEFEHLDT (1990) classified the enclaves into basalts and gabbros. However, some enclaves with gabbroic textures resemble the basaltic enclaves in their mineralogy and REE patterns. Thus, we do

Table 2. Modal composition of the enclaves (vol %).

Enclave	Group	Aug	Pig, Opx	Ol	Pl	Sil	Pho	Chr	Ilm	Rut	Zir	Bad	Tro	Met
4657	I-b	8.5	48.1		40.7	1.1	+	0.4	0.3	+		+	0.9	0.2
4671	I-b	9.4	44.1		41.1	4.2	0.1	0.4	0.3	+		+	0.2	0.1
4677	I-b	17.9	37.3		27.0	10.8	0.3	0.9	0.3	0.1		+	4.4	0.9
4678	I-b	11.5	39.5		41.9	5.5	0.1	0.7	0.3	0.3		+	0.1	+
4679	I-b	14.6	42.9		38.9	2.4	+	0.4	0.2	+		+	0.4	0.2
4683	I-b	13.6	29.7		53.5	2.0	0.1	0.5	0.1	+		+	0.5	0.1
4695	I-b	12.4	41.8		41.2	3.4	0.1	0.5	0.1	0.1		+	0.2	0.2
4669	I-f	10.4	45.8		38.1	5.1	0.1	0.3					0.3	0.1
4672	I-f	4.8	40.2		50.6	2.8	0.9	0.5					0.2	+
4674	I-f	8.4	39.0		48.0	3.8	0.3	0.3					0.3	+
4659	B		85.1				1.3	1.5	+	+			9.6	2.5
4689	B	10.5	37.4		21.8	16.3	2.1	1.9	0.3	0.1			7.8	1.8
4670-wh	B	0.2	63.4	23.5	0.1	+	0.3	1.6					6.9	4.0
4670-C1	B	1.3	96.2	1.8	+	+	+	0.6					0.1	+
4670-C3	B	+	15.5	69.0			0.1	1.3					8.8	5.3
4670-C4	B	+	34.0	45.9	+	+	+	0.8					12.2	7.1
4670-C9	B	1.4	80.9	9.5	0.8	+	0.7	3.0					2.8	0.8
4687	B	15.7	46.1		29.7	3.3	0.2	0.6	0.3	+	+		2.7	1.5

Group I-b: Ilm-bearing, I-f: Ilm-free, B: breccia, +: trace amount. 4670 wh: whole enclave, C1: orthopyroxene-rich clast, C3: olivine-rich clast, C4: olivine-orthopyoxene clast, and C9: orthopyroxene-olivine clast.

not classify the enclaves with the terms "basaltic" and "gabbroic".

The mineralogical and petrographic characteristics of the 38 enclaves are summarized in Table 1. There are 15 coarse-grained gabbroic ilm-free enclaves consisting mainly of pigeonite and plagioclase, 15 fine- to medium-grained ilm-bearing enclaves with ophitic to gabbroic textures, and 8 brecciated enclaves. Fourteen of these enclaves were selected for detailed SEM-petrography study (7 ilm-bearing, 3 ilm-free and 4 brecciated enclaves). Table 2 shows their mineral assemblages and modal abundances.

The brecciated enclaves include diogenitic breccias (Nos. 4659 and 4689) and an olivine-orthopyroxenite monomict breccia (No. 4670). The two diogenitic breccias include MgO-rich orthopyroxene (En_{74-65}). The olivine-orthopyroxenitic breccia consists mainly of olivine (Fo_{74-71}) and orthopyroxene (En_{78-75}). Pigeonite from the ilm-free enclaves is more enriched in MgO (En_{56-49}) than those from the ilm-bearing enclaves (En_{44-36}), and the mineral assemblages of these groups are also different. We found baddeleyite in all of the ilm-bearing enclaves, whereas the ilm-free enclaves contained none.

The fourteen enclaves do not appear to have suffered extensive shock melting or severe terrestrial weathering. These enclaves do not show any evidence of severe recrystallization or reduction reactions, as found in the silicate fraction in the host mesosiderite.

3.1. Ilm-free enclaves

All the ilmenite-free enclaves have gabbroic to granular textures. The silicate

phases in the ilm-free enclaves consist of low-Ca pyroxene, augite, plagioclase and silica mineral (mostly tridymite). Thin exsolution lamellae of augite in pigeonite are observed under the microscope. Thick bands of augite, 80–100 microns in width, commonly occur within pigeonite. Coarse-grained irregular-shaped augite also occurs in the peripheral parts of pigeonite. Silica minerals typically occur along the grain boundary between pigeonite and plagioclase. The abundance of opaque minerals is very low, and chromite and troilite, with rare amount of Fe-Ni metal, are observed.

Enclave 4669

This enclave has a coarse-grained gabbroic to granular texture (Photo 1). Low-Ca pyroxene in this enclave consists of pigeonite only.

Enclave 4672

This enclave has a coarse-grained gabbroic texture (Photo 2). Pigeonite always contains thick (>2 microns) and thin (<1 micron) lamellae of augite in a (001) direction (Photo 3). Most of the pigeonite is replaced by orthopyroxene in its peripheral parts (Photo 4). This replacement texture was first reported by IKEDA *et al.* (1990), and such replacements occur everywhere in the thin section. Phosphates (whitlockite) occur as irregular-shaped grains (20–30 microns) along the grain boundaries between pyroxene and plagioclase, or as spherical to irregular-shaped grains (<10 microns) in orthopyroxene.

Enclave 4674

This enclave has a coarse-grained gabbroic texture (Photo 5). Pigeonite shows replacement textures, and plagioclase abundantly contains tiny inclusions (1–20 microns in size) of silica mineral and/or pyroxene (predominantly pigeonite).

3.2. Ilm-bearing enclaves

The ilm-bearing enclaves have ophitic to gabbroic textures (Table 1). The silicate phases in the ilm-bearing enclaves consist of low-Ca pyroxene (predominantly pigeonite), augite, plagioclase and silica mineral. Exsolution lamellae of augite in the pigeonite are difficult to observe microscopically. Some augites occur as thick band (up to 80–90 microns in width) in pigeonite, in addition to isolated coarse-grained augite. Plagioclase commonly contains tiny inclusions (5–30 microns) which are pigeonite, augite and silica mineral. Some plagioclase appears to be dusty, and contains very fine inclusions (<1 micron) which are probably also pigeonite judging from qualitative analysis. Plagioclase shows a zonal growth structure as indicated by the distribution of dusty to tiny inclusions. However, most of the plagioclase in the ilm-bearing enclaves is homogeneous, as noted later. Silica minerals (mostly tridymite) occur abundantly in the interstices between pigeonite and plagioclase. Phosphates have a low abundance in all the ilm-bearing enclaves. They typically occur along grain boundaries between plagioclase and pigeonite (often with silica mineral). Opaque minerals also have a low abundance in the ilm-bearing enclaves. They are chromite and ilmenite with rutile, baddeleyite, troilite and Fe-Ni metal.

Enclave 4657

This enclave has a medium to fine-grained ophitic texture (Photo 6). Pigeonite in this enclave does not show any replacement texture by orthopyroxene. The pi-

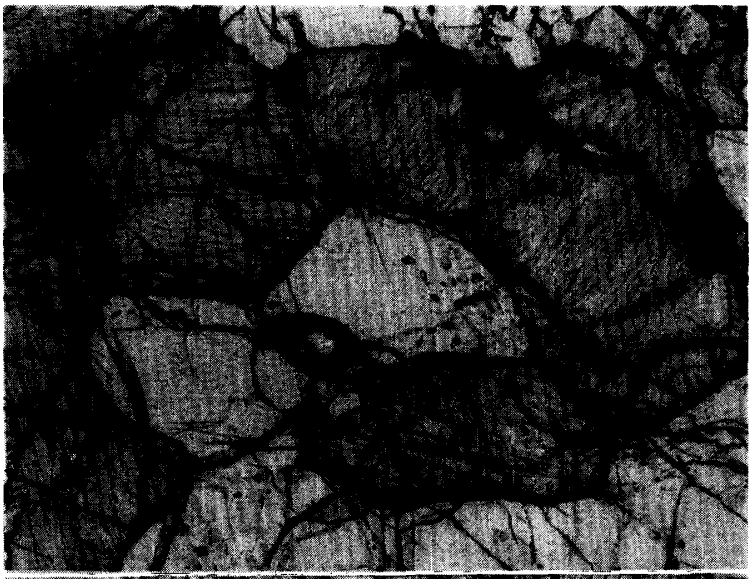

Photo 1. Ilm-free enclave 4669, consisting mainly of pigeonite (gray) and plagioclase (white). Transmitted light, open nicols, and width of 2 mm.

Photo 2. Ilm-free enclave 4672. Note that pigeonite is surrounded by orthopyroxene with abundant opaque minerals (black). Pigeonite is almost free of opaque minerals. Transmitted lignt, open nicols, and width of 2 mm.

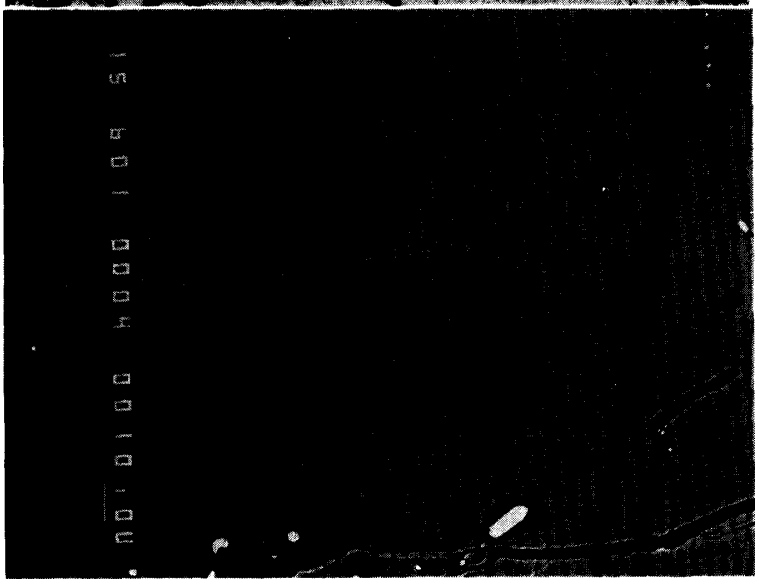

Photo 3. Augite lamellae (dark gray) in pigeonite (gray) in ilm-free enclave 4672. Note that pigeonite in the ilm-free enclaves includes both thin and thick augite lamellae. BSE image, and width of 200 microns.

Photo 4. Replacement texture of pigeonite (bright) by orthopyroxene (dark) in enclave 4672. Augite lamellae (bright) extend from pigeonite core to orthopyroxene mantle. Transmitted light, cross nicols, and width of 1 mm.

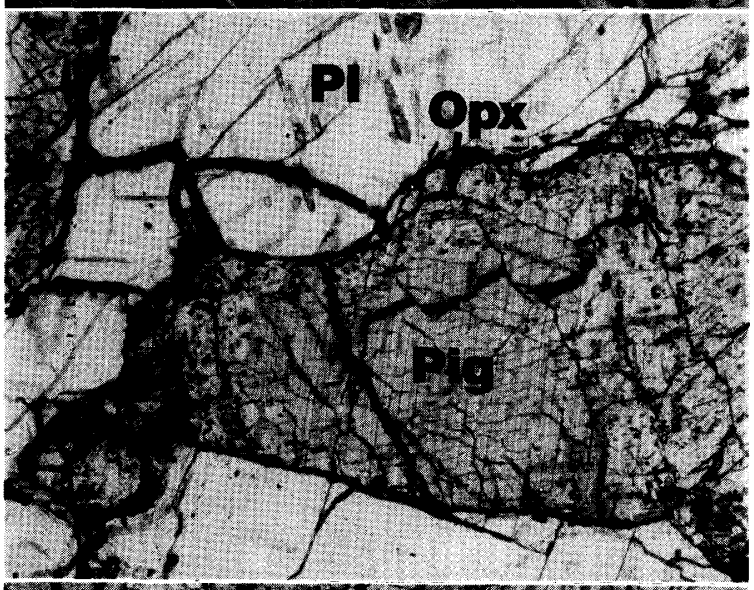

Photo 5. Ilm-free enclave 4674. Pigeonite is replaced by orthopyroxene with abundant opaque minerals. Transmitted light, open nicols, and width of 2 mm.

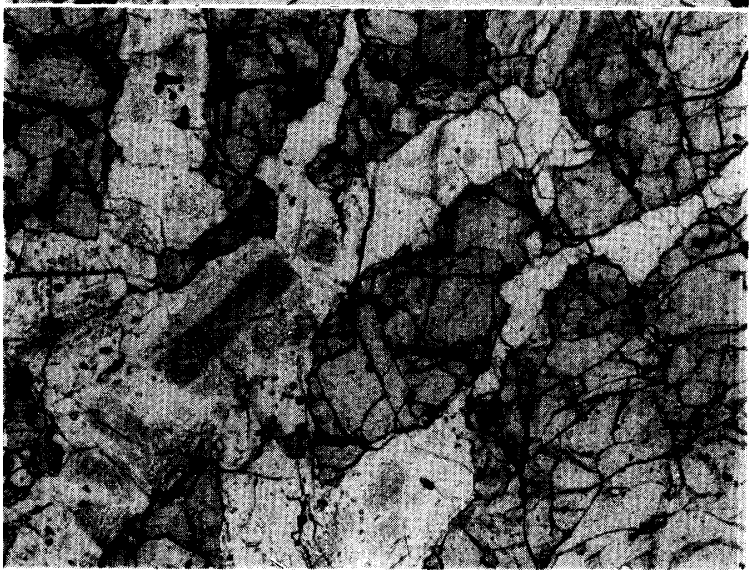

Photo 6. Ilm-bearing enclave 4657, consisting mainly of pigeonite (gray) and plagioclase (white). Some plagioclases appear to be dusty by the presence of very fine-grained inclusions. Transmitted light, open nicols, and width of 2 mm.

Photo 7. Abundant thin augite lamellae (dark) in pigeonite (bright) in ilm-bearing enclave 4657. BSE image, and width of 300 microns.

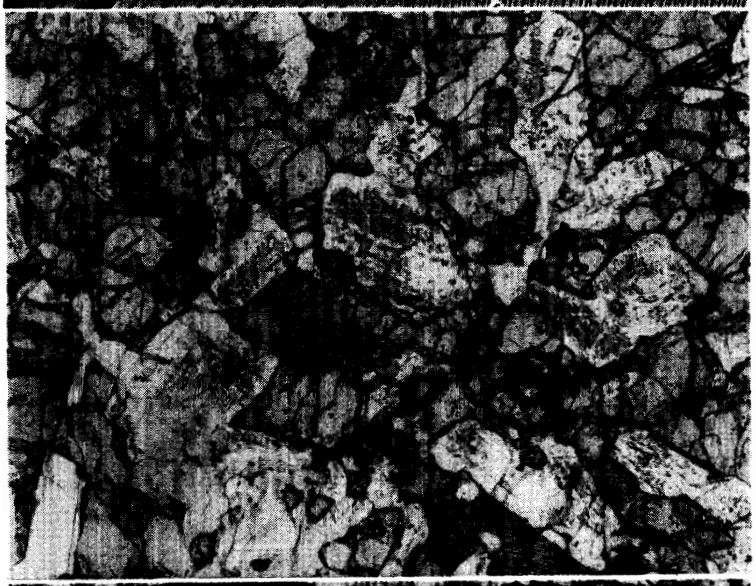

Photo 8. Ilm-bearing enclave 4671, consisting mainly of pigeonite (gray) and plagioclase (white). Transmitted light, open nicols, and width of 2 mm.

Photo 9. Ilm-bearing enclave 4677, consisting mainly of pigeonite (Pig), plagioclase (Pl) and silica mineral (Sil). Note that this enclave includes abundant opaque minerals (predominantly troilite). Transmitted light, open nicols, and width of 2 mm.

geonite includes very thin lamellae (usually less than 1 micron) which occur densely in comparison with those in the ilm-free enclaves (Photo 7).

Enclave 4671

This enclave has a medium-grained ophitic texture (Photo 8). Pigeonite does not show a replacement texture. Phosphate is very rare in this enclave.

Enclave 4677

This enclave also has a medium to fine-grained ophitic texture (Photo 9). It has a slightly monomict brecciated texture, and the brecciated parts are characterized by abundant troilite grains with fine-grained silicates. The boundaries between the brecciated parts and the other parts are not distinct. Pigeonite is not homogeneous (En_{50-40}), and magnesian pigeonite always occurs with troilite in the brecciated part. The other predominant pigeonite is FeO-rich (En_{40-44}). Pigeonite shows no replacement texture anywhere. A large amount of silica mineral and a small amount of plagioclase characterize this enclave (Table 2). Coarse-grained euhedral to subhedral silica minerals occur in association with pigeonite and plagioclase (Photo 10). Some of them occur as inclusions in pigeonite and plagioclase, which has a euhedral to subhedral lath structure (20–40 microns).

Enclave 4678

This enclave has a medium-grained granular to gabbroic texture (Photo 11). Pigeonite in this enclave shows a replacement texture by orthopyroxene. The replacements occur only in the peripheral parts of the thin section, and only a few grains show such a texture.

Enclave 4679

This enclave has a medium- to fine-grained ophitic texture (Photo 12). No replacement texture of pigeonite is encountered. Irregular-shaped phosphates occur in association with plagioclase, silica mineral and rarely ilmenite.

Enclave 4683

This enclave has a coarse-grained gabbroic to doleritic texture consisting mostly of irregular-shaped pigeonite and plagioclase (Photo 13). It contains a very coarse-grained plagioclase (megacryst), 1 cm in size.

Enclave 4695

This enclave has a medium-grained ophitic texture (Photo 14). A few pigeonites in the peripheral parts of the thin section show a replacement texture by orthopyroxene.

3.3. Olivine-orthopyroxenitic monomict enclave 4670

This enclave has a brecciated texture (Photo 15), and consists of fine- to coarse-grained orthopyroxene, olivine, troilite and chromite with minor phosphate, silica mineral, plagioclase, augite and Fe-Ni metal. The enclave consists of several clasts, *i.e.*, one orthopyroxene-rich clast, one olivine-rich clast, a few olivine-orthopyroxene clasts, and a fine-grained marginal part. Except for the marginal part, the boundaries between the clasts are not very clear. Table 2 gives the modal abundances of the whole of enclave 4670 and four of the clasts. Polymict diogenite is defined as containing more than 90% of orthopyroxenite (DELANEY *et al.*, 1983). The abundances of olivine (23.5 vol %) and orthopyroxene (63.4), thus, show that this enclave is an olivine-orthopyroxenite, not polymict diogenite. Although mesosiderite hosts

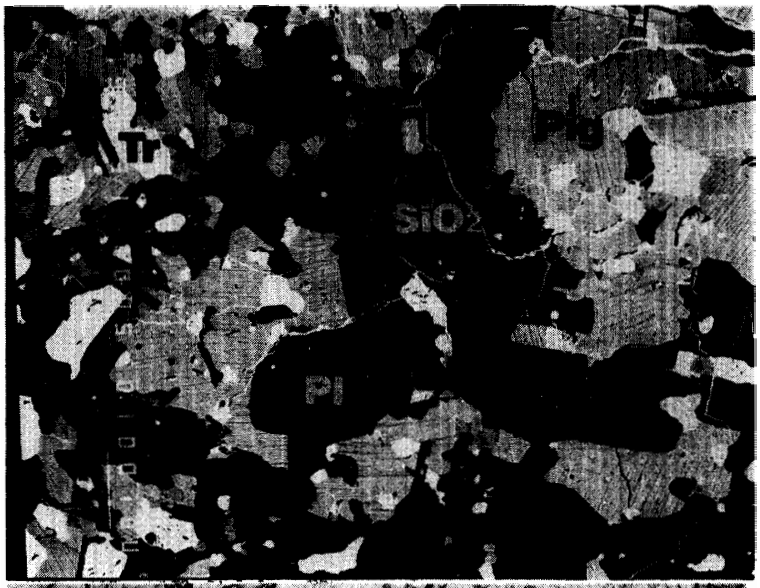

Photo 10. BSE image of enclave 4677. Note that euhedral to subhedral silica mineral occurs abundantly. Width of 900 microns.

Photo 11. Ilm-bearing enclave 4678. Transmitted light, open nicols, and width of 2 mm.

Photo 12. Ilm-bearing enclave 4679. Transmitted light, open nicols, and widh of 2 mm.

Photo 13. Ilm-bearing enclave 4683, consisting of coarse-grained plagioclase (white) with pigeonite (gray). Transmitted light, open nicols, and width of 4.5 mm.

Photo 14. Ilm-bearing enclave 4695. Transmitted light, open nicols, and width of 2 mm.

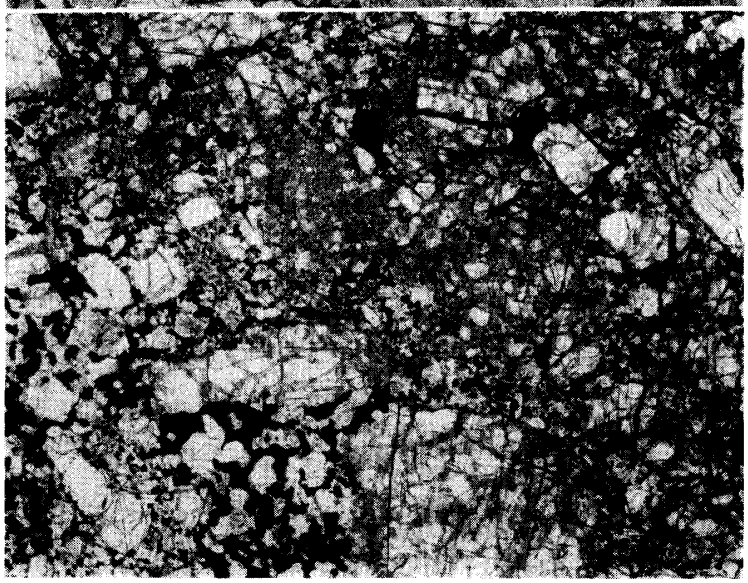

Photo 15. Olivine-orthopyroxenitic brecciated enclave 4670, consisting of many clasts and fine to coarse-grained silicate fragments with abundant opaque minerals. Olivine-rich clast occurs in lower-left corner. Transmitted light, open nicols, and width of 4.5 mm.

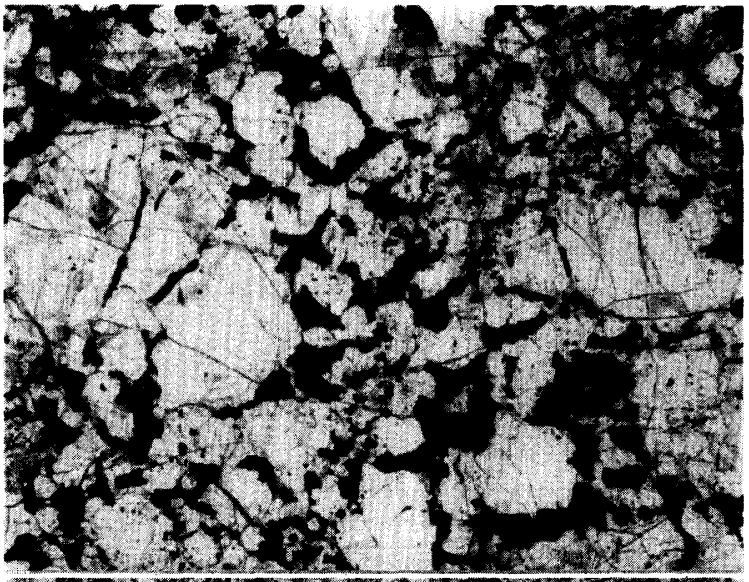

Photo 16. Olivine-rich clast in enclave 4670, consisting mainly of olivine (white) and troilite (black). Transmitted light, open nicols, and width of 2 mm.

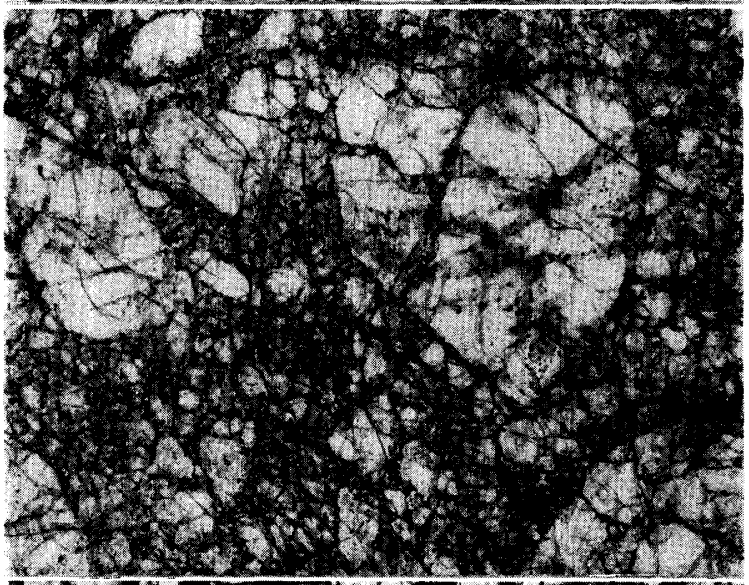

Photo 17. Orthopyroxene-rich clast in enclave 4670, consisting mostly of fine- to coarse-grained orthopyroxene fragments. Transmitted light, open nicols, and width of 2 mm.

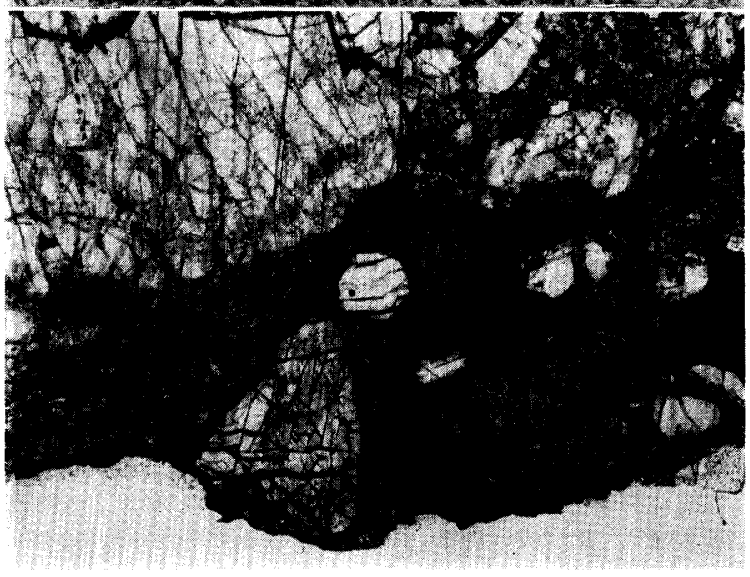

Photo 18. Marginal part of enclave 4670. This fine-grained aggregate, with silicate and opaque fragments, occurs along one side of the thin section. Transmitted light, open nicols, and width of 2 mm.

include a large amount of olivine clasts (MITTLEFEHLDT, 1979), this is the first discovery of an olivine-rich orthopyroxenitic enclave. Orthopyroxene in all the clasts does not include any lamellae of augite. Opaque minerals (troilite, Fe-Ni metal and chromite) are distributed heterogeneously, and some clasts are enriched in troilite and metal. The total abundance of opaque minerals is much higher than in the ilm-bearing and ilm-free enclaves.

The olivine-rich clast (C3) consists of olivine (69.0 vol %) with small amounts of orthopyroxene, phosphate, chromite, troilite and Fe-Ni metal (Photo 16). Fine-grained augite occurs rarely in this clast, but plagioclase and silica mineral appear to be absent. The orthopyroxene-rich clast (C1) consists mostly of orthopyroxene (96.2%) with rare olivine, plagioclase, augite and silica mineral (Photo 17). Opaque minerals are very poor in this clast. Olivine-orthopyroxene clasts consist of olivine and orthopyroxene with phosphate, plagioclase, augite, silica mineral, chromite, troilite and metal. Some orthopyroxene includes tiny spherical inclusions of olivine. The abundances of these minerals vary widely in these clasts. Plagioclase, silica mineral and augite are less than 10 microns in size. They occur in the interstices between orthopyroxenes. Phosphates also occur along orthopyroxene or olivine grains.

The fine-grained portion occurs along the margin of the thin section (Photo 18). It consists mainly of fine-grained groundmass similar to devitrified glass, with small amounts of fragmental orthopyroxene, opaque minerals, phosphate and silica mineral. The groundmass consists of fine-grained low-Ca pyroxene and plagioclase. One coarse olivine fragment occurs in this part. This olivine is surrounded by a corona of orthopyroxene and chromite, which resembles the coronas in mesosiderite hosts (NEHRU *et al.*, 1980b).

3.4. Diogenitic breccia

Enclave 4659

This is a fine- to coarse-grained monomict breccia consisting mainly of orthopyroxene (85.1 vol %) with phosphate, chromite, ilmenite, rutile, troilite and Fe-Ni metal (Photo 19). Plagioclase, augite and silica mineral do not appear to occur in this enclave. Orthopyroxenes have no lamellae of augite. A large amount of phosphates characterizes the diogenitic enclaves. Phosphates, 10 to 60 microns in size, occur within the coarse-grained orthopyroxene or with the fine-grained pyroxene. The abundance of opaque minerals, especially troilite, is very high.

Enclave 4689

This enclave has a fine-grained brecciated texture (Photo 20), and consists of orthopyrocxne with augite, plagioclase, silica mineral, phosphate, chromite, ilmenite, rutile, troilite and Fe-Ni metal. The enclave includes many small clasts with a basaltic texture. Although orthopyroxene does not include lamellae, they often contain finegrained augite with very thin (001) lamellae. The abundance of opaque minerals, phosphate and silica mineral is very high. One coarse-grained orthopyroxene fragment occurs in the marginal part of the thin section, which is more enriched in MgO (En_{73} in core, En_{65} in rim) than the other homogeneous orthopyroxene (En_{65}, average).

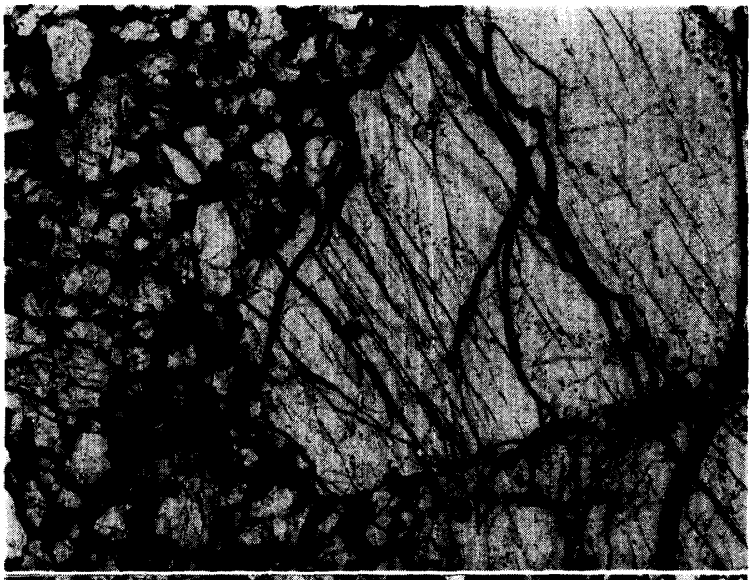

Photo 19. Diogenitic enclave 4659, consisting of orthopyroxene fragments and opaque minerals (mostly troilite). Transmitted light, open nicols, and width of 2 mm.

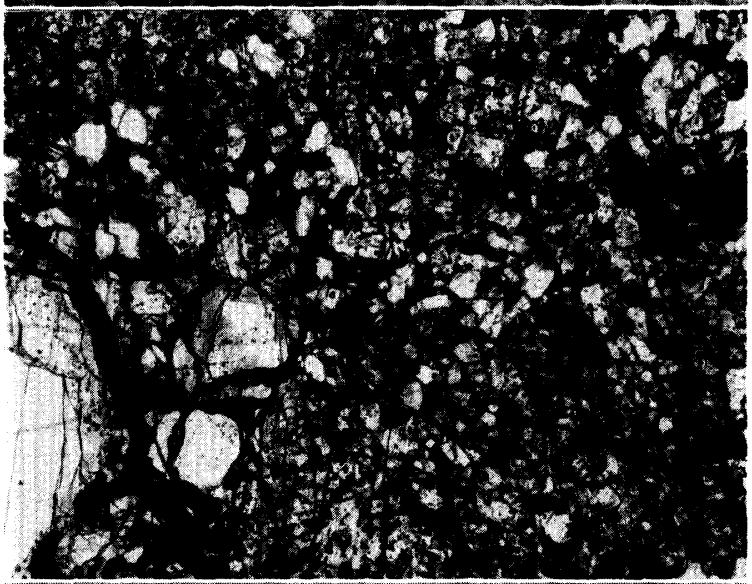

Photo 20. Diogenitic enclave 4689, consisting of fine-grained orthopyroxene fragments with plagioclase, silica mineral, phosphate and abundant troilite. A magnesian orthopyroxene coarse fragment occurs on the left side of this photograph. Transmitted light, open nicols, and width of 2 mm.

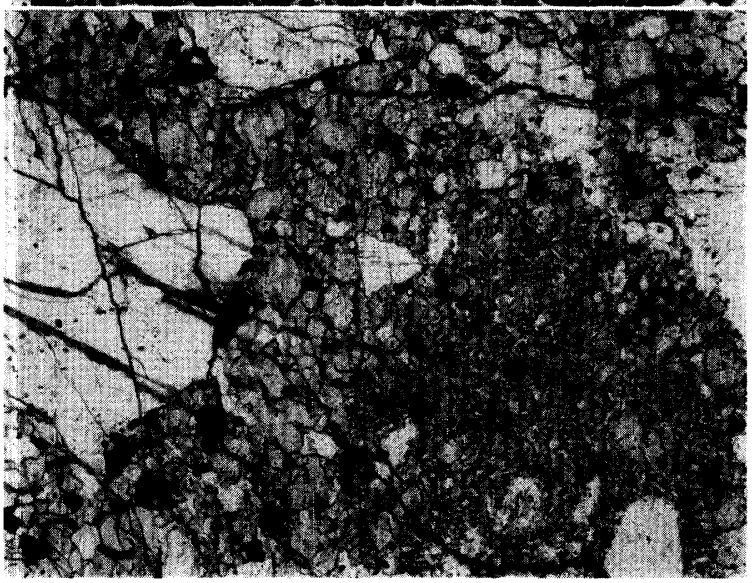

Photo 21. Recrystallized brecciated enclave 4687, consisting of clasts and silicate fragments of various sizes. Transmitted light, open nicols, and width of 2 mm.

3.5. Recrystallized brecciated enclave 4687

This enclave has a recrystallized brecciated texture (Photo 21), and consists of many clasts and mineral fragments of various grain sizes. Some clasts have ophitic textures and others have gabbroic textures. One clast consists of augite and silica mineral only, and this enclave contains several zircon grains. Although pigeonite is the predominant pyroxene, several coarse-grained orthopyroxene fragments, with augite blebs, occur. These fragmental orthopyroxenes differ from the replacing orthopyroxene around pigeonite, as noted above. Orthopyroxene is more enriched in MgO (En_{51-58}) than pigeonite (En_{44-51}). Plagioclase is heterogeneous in composition (An_{90-96}), and few coarse plagioclase fragments are enriched in CaO.

4. Mineralogy

4.1. Olivine

Table 3 gives representative compositions of olivine and the other silicate minerals. Olivine was found only in olivine-orthopyroxenitic brecciated enclave 4670. The olivine and orthopyroxene in this enclave have a slight compositional heterogeneity in each clast, being Fo_{74-71} and En_{78-75} respectively. The composition of the olivine overlaps with that of olivine (Fo_{73-62}) in the Vaca Muerta mesosiderite (DELANEY *et al.*, 1980). The average FeO/MnO ratio of the olivine is 35.6, which is within the range of mesosiderite olivine given by DELANEY *et al.* (1980). Olivine and orthopyroxene in the marginal part of enclave 4670 are enriched in FeO (Fo_{65-63} and En_{69-64}).

4.2. Pyroxene

Pyroxene is the most common phase in enclaves of all types. Orthopyroxene is the predominant phase in magnesian olivine-orthopyroxenite and diogenitic breccias. Pigeonite is the predominant phase in the ilm-bearing and ilm-free enclaves, although orthopyroxene occurs replacing pigeonite in these enclaves. Besides as thin lamellae in pigeonite, augite occurs as isolated coarse grains and as thick bands, within pigeonite, in many enclaves. Except for some breccias, every enclave contains homogeneous pyroxene. The TiO_2 content of the pyroxene distinguishes the ilm-bearing enclaves (0.2–0.5 wt %) from the ilm-free enclaves (<0.2 %).

The most striking feature of the pyroxene is the replacement of pigeonite by orthopyroxene. Most of the pigeonite in the ilm-free enclaves is completely surrounded by orthopyroxene. Fourteen of the fifteen ilm-free enclaves studied have such a texture. On the other hand, pigeonite occurring in the marginal parts is replaced by orthopyroxene in the ilm-bearing enclaves. Only 7 of the 15 ilm-free enclaves include such orthopyroxenes. The occurrences and abundances of replacing orthopyroxene differ between the two types of enclaves. We observed these replacement textures, in detail, using back-scattered electron (BSE, hereafter) images.

Ilm-free enclaves (Photo 22)

Pigeonite and replacing orthopyroxene have different lamellar textures. Although both pigeonite and orthopyroxene include common, thick, lamellae of augite along the (001) direction (5–8 microns in width), pigeonite further includes many

Table 3. Representative compositions of augite (aug), pigeonite (pig), orthopyroxene (opx), plagioclase (pl) and olivine (ol) (wt%).

Enclave	Group		SiO_2	TiO_2	Al_2O_3	Cr_2O_3	FeO	MnO	MgO	CaO	Na_2O	K_2O	Total
4657	I-b	pl	45.35	0 00	34 32	0 00	0 13	0 07	0 04	18 45	1.07	0.06	99.49
4657	I-b	aug	49 90	0 71	0 88	0 34	19.12	0.72	9.96	17.60	0.09	0.00	99.32
4657	I-b	pig	48.06	0.33	0 37	0 13	36 04	1.36	11.76	1.88	0.06	0.00	99.99
4671	I-b	pl	44.82	0.00	34.07	0 00	0.22	0.00	0.04	18.42	1.21	0.00	98.78
4671	I-b	aug	49.25	0.75	0 87	0 31	23.11	0 95	10.78	13.63	0.09	0.00	99.74
4671	I-b	pig	49.20	0.34	0 40	0.11	33.16	1.28	12.22	3.86	0.04	0.00	100.61
4677	I-b	pl	45.19	0.00	34.83	0 05	0 22	0.00	0.04	18.42	1.07	0.04	99.86
4677	I-b	aug	49.71	0.83	1.63	0.52	14.41	0.66	12.07	19.02	0.06	0.00	98.91
4677	I-b	pig	50.35	0.36	0 37	0.28	28.39	1.06	16.11	2.87	0.00	0.00	99.79
4677	I-b	pig	49.59	0.28	0 31	0 25	32.10	1.54	13.76	1.75	0.02	0.00	99.60
4678	I-b	pl	45.58	0.00	34.85	0 00	0.16	0.00	0 04	18.45	1.21	0.00	100.29
4678	I-b	aug	51.50	0.63	0 79	0 31	11.01	0.52	14.14	21.16	0 07	0.00	100.13
4678	I-b	opx	51.45	0.50	0 52	0 26	24 87	1.22	19.39	1.82	0.00	0.00	100.03
4678	I-b	pig	49.10	0.45	0.32	0.18	33.87	1.29	12.73	1.00	0.00	0.00	98.94
4679	I-b	pl	45.15	0.05	34.76	0.00	0 25	0.00	0.04	18.54	1.13	0.00	99.92
4679	I-b	aug	50.40	0.72	0 92	0.38	15.40	0.74	11.17	19.33	0.08	0.00	99.14
4679	I-b	pig	49.14	0.35	0.31	0.10	34.69	1.24	12.27	1.88	0.03	0.00	100.01
4683	I-b	pl	45.57	0.07	34.17	0 07	0.28	0.13	0.03	18.27	1.43	0.10	100.11
4683	I-b	aug	50.08	0.69	1.27	0.47	16.58	0.55	11.46	18.78	0.09	0.00	99.97
4683	I-b	pig	49.79	0.32	0.40	0 23	32 52	1.33	13.39	1.66	0.00	0.00	99.64
4695	I-b	pl	44.79	0.00	34.56	0.00	0 27	0.28	0.03	18 96	1.08	0.00	99.97
4695	I-b	aug	51.57	0.61	0.70	0.29	13.22	0.83	13.50	19.81	0.09	0.00	100.62
4695	I-b	opx	51.64	0.37	0.41	0.16	26.51	1.12	17.84	1.56	0.00	0.00	99.61
4695	I-b	pig	50.20	0.50	0.27	0.16	30.81	1.34	15.03	0.96	0.00	0.00	99.26
4669	I-f	pl	44.30	0.06	35.30	0.04	0.10	0.00	0.03	19.43	0.76	0.00	100.04
4669	I-f	aug	51.22	0.22	0.95	0.58	12.44	0.37	12.83	20.37	0.06	0.00	99.04
4669	I-f	pig	50.41	0.06	0.26	0.31	29.05	1.13	17.41	0.92	0.00	0.00	99.55
4672	I-f	pl	43.75	0.10	35.74	0 08	0.10	0.00	0.06	19.54	0.59	0.00	99.96
4672	I-f	aug	52.28	0.15	0.64	0.40	10.20	0.60	14.19	21.47	0.06	0.00	99.99
4672	I-f	opx	50.88	0.07	0.33	0.34	24.68	0.67	20.84	1.47	0.00	0.00	99.28
4672	I-f	pig	51.92	0.04	0.37	0.32	26.57	1.17	19.53	0.87	0.00	0.00	100.79
4674	I-f	pl	44.30	0.00	35.60	0.04	0.15	0.16	0.00	18.60	0.69	0.04	99.58
4674	I-f	aug	51.58	0.24	0.65	0.58	9.56	0.67	15.63	20.33	0.06	0.00	99.30
4674	I-f	opx	52.60	0.15	0.26	0.10	24.68	1.14	19.88	1.72	0.00	0.00	100.53
4674	I-f	pig	50.55	0.00	0.35	0.35	27.68	1.44	18 62	1.24	0.00	0.00	100.23
4659	B	opx	53.31	0.27	0.52	1.43	16 97	0.56	25.30	0.83	0.02	0.00	99.21
4689	B	pl	46.92	0.00	33.36	0.00	0 24	0.00	0 06	17.46	1.51	0.04	99.59
4689	B	aug	51.08	0.70	0.90	0.39	8.74	0.54	14.62	21.77	0.05	0.00	98.79
4689	B	opx	53.39	0.31	0.55	0.27	20.17	0.85	23.38	1.49	0.00	0 00	100.41
4670	B	ol	37.30	0.06	0.00	0.09	26.07	0.62	35.58	0 00	0 00	0.00	99.72
4670	B	pl	42.98	0.00	35.47	0.04	0.59	0.00	0 03	19.04	0.31	0.00	89.46
4670	B	aug	53.95	0.15	0.15	0.27	5.09	0.25	16.67	23.17	0.05	0.00	99.75
4670	B	opx	53.45	0.11	0.62	0.53	14.43	0.58	28.30	1.03	0.03	0.00	99.08
4687	B	pl	45.71	0.14	34.21	0.00	0.43	0.00	0.02	17.58	1.13	0.00	99.22
4687	B	aug	50.75	1.30	1.68	0.55	9.04	0.55	15.27	20.42	0.09	0.00	99.65
4687	B	opx	52.05	0.56	0.43	0.22	23.98	0.86	19.82	1.50	0.00	0.00	99.42
4687	B	pig	49.73	0.26	0.41	0.23	31.97	1.05	15.09	1.10	0.00	0.00	99.84

Group I-b: Ilm-bearing, I-f: Ilm-free, B: breccia.

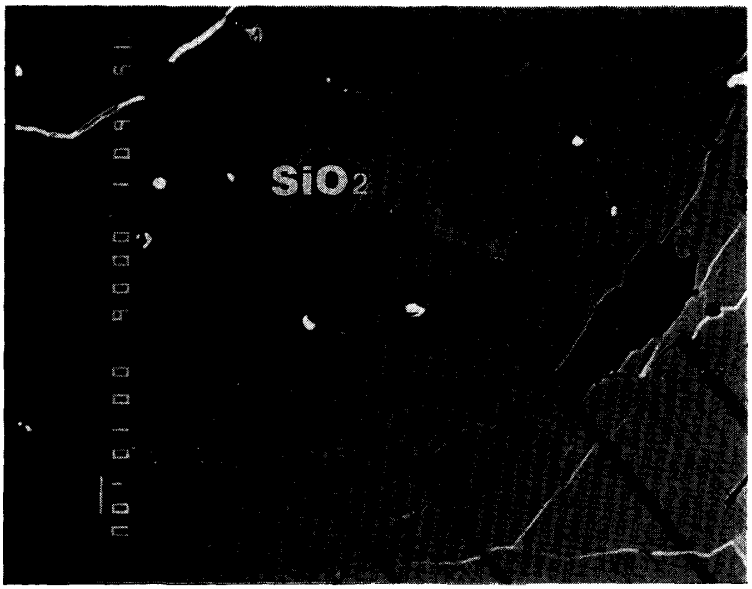

Photo 22. BSE image of replacement texture of pigeonite (Pig) by orthopyroxene (Opx) in ilm-free enclave 4672. Pigeonite and orthopyroxene include common thick augite lamellae (Aug). Pigeonite further includes thin lamellae of (001) direction, and orthopyroxene includes several thin lamellae of (100) direction. Silica mineral and troilite occur in the orthopyroxene. Note that the phosphate (whitlockite) and silica mineral assemblage occurs just cutting augite lamella. Width of 220 microns.

Photo 23. BSE image of replacement texture of pigeonite (Pig) by orthopyroxene (Opx) in ilm-bearing enclave 4678. The orthopyroxene includes augite with bleb shape, troilite and silica mineral. Augite lamellae in pigeonite do not extend into the orthopyroxene. Width of 220 microns.

thin (below 1 micron) lamellae along the (001) direction. On the other hand, orthopyroxene often includes thin lamellae along the (100) direction, up to 1 micron in width. Thick augite lamellae rarely include lamellae of (001) direction. In enclave 4674 they are not distinct. At ahy rate, the replacing orthopyroxene includes larger amounts of silica mineral and troilite than pigeonite (Photo 3), as noted by IKEDA *et al.* (1990). In addition, fine-grained phosphates (always REE-free whitlockite) typically occur cutting augite lamellae in orthopyroxene (Photo 22). They are 5 to 10 microns in size and have spherical to irregular shapes, and frequently coexist with silica mineral and troilite. Such phosphates were not encountered in pigeonites.

Ilm-bearing enclaves (Photo 23)

Replacing orthopyroxene does not contain (100) lamellae, but contains abundant augite, troilite, and silica minerals with small amounts of chromite, phosphate and

Fe-Ni metal. However, augite occurs as bleb-shaped grains, which differ from those in the ilm-free enclaves. Augite blebs often contain very thin (001) lamellae. Although pigeonite contains thin (001) lamellae of augite, these lamellae rarely extend to orthopyroxene. Thus, orthopyroxene-pigeonite assemblages in the ilm-free and ilm-bearing enclaves are clearly different from one another in lamellar texture as well as in occurrence and abundance.

Chemical relationships between pigeonite and orthopyroxenes

Replacing orthopyroxene is more enriched in MgO than pigeonite (Tables 1 and 3). Orthopyroxene in the ilm-bearing enclaves is considerably more magnesian than the pigeonite. Orthopyroxene and pigeonite often have weak chemical zoning within the peripheral parts, from MgO-rich to FeO-rich toward the boundary. For example, orthopyroxene in ilm-free enclave 4674 changes in composition from En_{62} to En_{58} near pigeonite, and pigeonite changes in composition from En_{54} to En_{56} near orthopyroxene. The CaO content of orthopyroxene is slightly, but systematically, higher than that of coexisting pigeonite, *e.g.*, 1.3–1.8 wt% and 0.8–1.0 in ilm-free enclave 4674, and 1.6–1.8 and 0.8–1.1 in ilm-bearing enclave 4695, respectively. MnO prefers pigeonite to orthopyroxene, *e.g.*, 1.2–1.4 and 1.0–1.2 in enclave 4674, and 1.3–1.4 and 1.1–1.3 in enclave 4695, respectively. This preference of MnO for pigeonite is consistent with HEWINS (1979).

4.3. Plagioclase

Plagioclase is one of the predominant minerals in most of the enclaves. However, it is absent in diogenitic enclave 4659 and has a very low abundance in olivine-orthopyroxenitic enclave 4670. Most plagioclase is homogeneous, except for very weak zoning from a calcic core to a sodic rim in a few grains. As noted above, plagioclase in some breccias is heterogeneous in composition. Plagioclase in the ilm-bearing enclaves is more sodic ($An_{87.6-92.3}$) than that in the ilm-free enclaves ($An_{92.1-95.8}$). An olivine-orthopyroxenitic breccia contains very calcic plagioclase (An_{97-98}), whereas plagioclase in the fine-grained marginal part is more enriched in Na_2O (An_{91-85}).

4.4. Silica mineral

Silica minerals occur in all enclaves, whereas they are rare or absent in the olivine-orthopyroxenite enclave 4670 and diogenitic breccia enclave 4659. Coarse- to medium-grained silica minerals are tridymite. They typically occur in the interstices between plagioclase and pyroxene grains, whereas some occur as euhedral to subhedral coarse grains. Such phenocrystic grains are especially common in ilm-bearing enclave 4677 (Photo 10).

4.5. Phosphates

The abundances of phosphates vary widely among different enclaves. Brecciated enclaves contain a large amount of phosphates. Their abundances in the ilm-free enclaves are higher than those in the ilm-bearing enclaves. The breccia and ilm-free enclaves contain only whitlockite. On the other hand, the ilm-bearing enclaves contain predominantly whitlockite and rare F-apatite. CFP-phases (Ca-, Fe- and

Table 4. Representative compositions of whitlockite (whi), apatite (apa) and Ca-Fe-P-phase (CFP) (wt%).

Enclave	Group		F	Cl	Y_2O_3	Ce_2O_3	Nd_2O_3	Na_2O	P_2O_5	MgO	CaO	MnO	FeO	"O=F, Cl"	Total
4657	I-b	whi	0.43	0.03	0.45	0.66	0.42	1.99	45.74	2.57	44.80	0.19	2.21	0 19	99.30
4671	I-b	apa	4.06	0.65	0 00	0.09	0.00	0.02	42.04	0.01	53.40	0.11	0 45	1 86	98 97
4671	I-b	CFP	0.39	0.02	1.03	1.28	0 72	0.75	31.98	1.28	31.02	0.26	4 07	0 16	72 64
4671	I-b	CFP	0.26	0.04	0.80	1.59	0.96	0.27	30.44	1.62	1.88	0.25	33 43	0 12	71.42
4677	I-b	whi	0 58	0.00	0 03	0.03	0.07	1.70	45.20	3.57	48.72	0.11	0 68	0 25	100 44
4678	I-b	apa	3.78	0.22	0.04	0.03	0 01	0.02	40.93	0.01	53.63	0.05	0.65	1 64	97.73
4678	I-b	whi	0.74	0.03	0.57	0.21	0.03	1.77	45.82	3.62	46.78	0 28	0 91	0.32	100.44
4679	I-b	whi	0.39	0 00	0.09	0.10	0.08	1.99	44.43	3.10	47.06	0 16	1.11	0 16	98 35
4683	I-b	apa	4.02	0.12	0.00	0.00	0.01	0.00	42.30	0.02	55.09	0 15	0 24	1.72	100 23
4683	I-b	whi	0.43	0 00	0.21	0.04	0.09	1.77	44.93	3.20	47.80	0.20	1 29	0.18	99.78
4695	I-b	whi	0.48	0 02	0.21	0.17	0.07	1.67	45.21	2.65	47.02	0.12	1.83	0.22	99 23
4669	I-f	whi	0.36	0.00	0 00	0.07	0.00	2.18	45.90	3.23	47.43	0.24	1.21	0.15	100 47
4672	I-f	whi	0.42	0.04	0.01	0.05	0.00	1.19	45.28	3.37	46.19	0.13	1.51	0.19	98 00
4674	I-f	whi	0 69	0.01	0 00	0.05	0 11	2.30	45.19	3.62	47.24	0.21	0 29	0 29	99.42
4687	B	whi	0 53	0 00	0.26	0.17	0.11	1.56	41.87	3.03	47.08	0.21	3.96	0.23	98.55
4659	B	whi	0.71	0.00	0 00	0.06	0.03	1.26	45.17	3.67	47.08	0 31	0.81	0 30	98.80
4689	B	whi	0 51	0.02	0 01	0.05	0.00	1.61	45.80	3.67	46.88	0 14	0.66	0 23	99.12
4670	B	whi	0 65	0 01	0.00	0.00	0.00	1.33	47147	3.64	46.90	0.08	0.67	0.27	100.48

Group I-b: Ilm-bearing, I-f: Ilm-free, B: breccia.

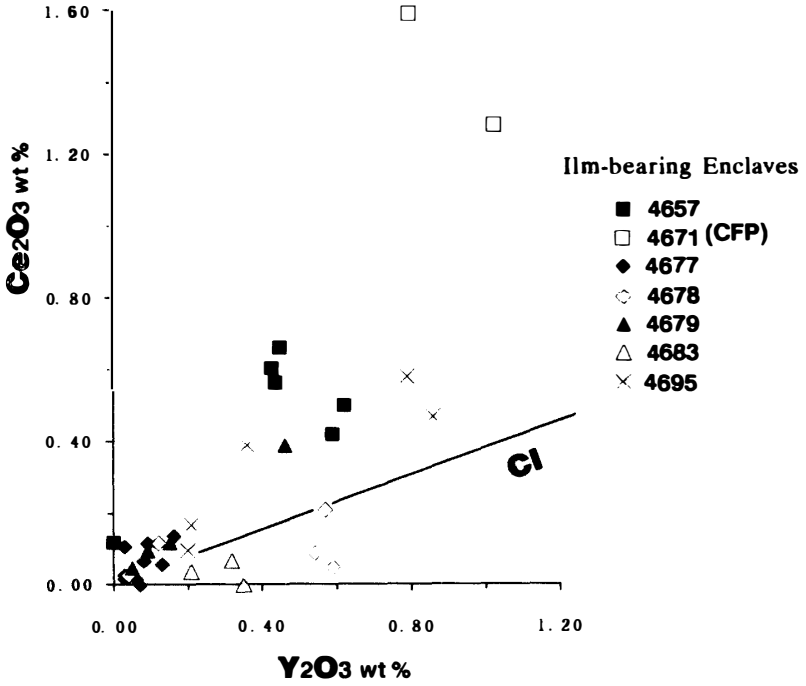

Fig. 1. Concentration of Ce_2O_3 and Y_2O_3 of phosphates in the ilm-bearing enclaves. Phosphates in No. 4671 are Ca-Fe-P-phase. and others are whitlockites. The straight line (CI) shows the ratio of thses elements in CI chondrites (ANDERS and GREVESSE, 1989).

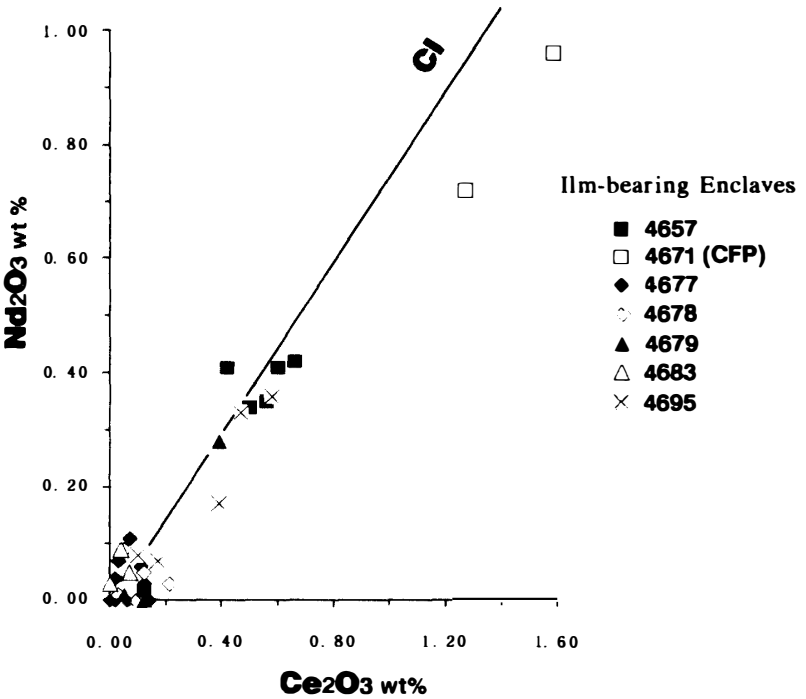

Fig. 2. Concentration of Ce_2O_3 and Nd_2O_3 of phosphates in the ilm-bearing enclaves. The straight line (CI) shows the CI chondrite ratio (ANDERS and GREVESSE, 1989).

P-bearing non-stoichiometric phosphates) reported by IKEDA *et al.* (1990), aslo occur in ilm-bearing enclave 4671. They are interpreted to be weathering products altered from whitlockites.

Table 5. Representative compositions of chromites (chr), ilmenites (ilm) and rutiles (rut) (wt%).

Enclave	Group		SiO_2	TiO_2	Al_2O_3	Cr_2O_3	FeO	MnO	MgO	ZnO	V_2O_3	CaO	Nb_2O_5	Total
4657	I-b	chr	0.09	5.45	8.63	47.47	36.04	0.46	0.72	0 07	0.65	0.07	0.10	99.76
4657	I-b	ilm	0.08	52.80	0 01	0.71	44.42	0.96	0 76	0 00	0.00	0.00	0.00	99.74
4671	I-b	chr	0.07	9.08	7.49	43 98	36.82	0.58	0.95	0.03	0.69	0 02	0.00	99.73
4671	I-b	ilm	0 04	53.20	0.01	0.11	44.46	0.91	1.00	0 00	0 00	0 05	0.06	99.84
4561	I-b	rut	0.00	99.93	0.04	0.07	0.74	0.12	0.00	0.00	0.00	0.00	0.07	100.97
4677	I-b	chr	0.02	7.76	7.07	46.60	35.31	0.82	0.94	0.00	0 67	0.05	0 00	99.27
4677	I-b	ilm	0 03	53.28	0.02	0.25	44.43	1.67	1.14	0.10	0.00	0 00	0 00	101.00
4677	I-b	rut	0.30	95.89	0.04	0.16	2.68	0.02	0.05	0 00	0.12	0 02	0.58	99.86
4678	I-b	chr	0.01	3.69	6.99	54.49	32.03	0.94	0.72	0 11	1.02	0 02	0 00	100.04
4678	I-b	ilm	0.04	52 94	0.02	0.37	42.83	1.34	1.54	0.00	0 00	0 00	0 00	99.13
4678	I-b	rut	0.04	98.35	0.02	0.06	0.21	0.15	0.00	0.00	0 00	0 00	0.15	98.98
4679	I-b	chr	0.00	7.33	6.72	45.43	39.42	0.88	0.31	0.00	0 61	0 00	0.00	100.70
4679	I-b	ilm	0.00	53.80	0 01	0.06	45.31	1.23	0.71	0.00	0.00	0.00	0 00	101.12
4697	I-b	rut	0 00	100.50	0.00	0.10	0.59	0.00	0.00	0 00	0 00	0 00	0 00	101.19
4683	I-b	chr	0.06	6.30	7.14	47.31	35.51	0.83	1.49	0 00	0 83	0 02	0.00	99.50
4683	I-b	ilm	0.01	53.77	0.02	0 12	43 03	1.76	1.79	0.00	0 00	0 02	0.05	100.57
4683	I-b	rut	0.06	99.94	0 00	0 00	0 21	0.06	0.00	0.00	0 00	0 00	0.10	100.37
4695	I-b	chr	0.05	5.28	7.81	50 04	33 37	0.62	0.93	0.00	0.84	0 01	0 00	99.04
4695	I-b	ilm	0.02	54.51	0.00	0 00	43.34	1.23	1.12	0.00	0 00	0 00	0 02	100.29
4695	I-b	rut	0.00	100 06	0.03	0.15	0.42	0.03	0.00	0 00	0.00	0 00	0.18	100.99
4669	I-f	chr	0.12	1.12	10 03	53.93	32.35	0.52	1.74	0 00	0.56	0 00	0.00	100 37
4672	I-f	chr	0 07	2.06	8.72	54.09	30.37	1.08	1.66	0 02	0.54	0.07	0.00	98 68
4672	I-f	chr	0.12	0.09	9.57	55.29	30.06	1.03	1.95	0 00	0.79	0 07	0 06	99 05
4674	I-f	chr	0.05	1.89	8.74	53.46	31.41	1.09	1.08	0 00	0.47	0 01	0 08	98.30
4674	I-f	chr	0.06	0.59	10.75	53.95	29.83	0.77	1.87	0.07	0 60	0 02	0.00	98.54
4659	B	chr	0.03	5.49	0.03	60.46	27.05	1.66	1.74	0 14	1.76	0 07	0.00	98.58
4659	B	chr	0.10	1.82	10.31	53.67	28.27	1.11	3.18	0.00	0 54	0 03	0 00	99.03
4659	B	ilm	0.02	53.40	0.01	0.63	35.95	5.38	4.10	0.02	0.00	0 00	0 00	99 51
4659	B	ilm	0.04	55.79	0.03	0.03	25.52	13.78	4.75	0.00	0 00	0 00	0.05	100.12
4659	B	rut	0.00	98.03	0.02	0.10	1.50	0.00	0.00	0.00	0 00	0.00	0 05	99.76
4689	B	chr	0.02	4.52	0.62	62.68	29.11	1.50	1.53	0.00	0 65	0.00	0.00	100.63
4689	B	chr	0.00	3.12	9.23	52.55	29.71	1.11	2.80	0.03	0 52	0.06	0.00	99.13
4689	B	ilm	0.00	53.80	0.00	0.81	34.92	6.54	3.58	0.00	0 00	0 00	0 00	99.65
4689	B	rut	0.01	98.61	0.36	0.40	0.40	0.00	0.00	0 00	0.00	0.00	0.33	99.75
4670	B	chr	0.12	0.97	16.02	47.37	29.37	0.77	3.58	0.00	0 28	0.01	0.04	98.57
4670	B	chr	0.06	1.77	8.32	53.67	31.52	0.98	1.67	0.00	0.46	0.40	0.03	98.88
4687	B	chr	0.03	6.41	7.52	47.13	36.85	0.70	0.95	0.00	0.84	0.00	0.00	100 46
4687	B	ilm	0.01	53.91	0.02	0.17	43.52	1.17	1.72	0.09	0.00	0.00	0 00	100.61
4687	B	rut	0.02	95.51	0.04	0.83	1.80	0.02	0.00	0.05	0.00	0.00	1.87	100.27

Group I-b: Ilm-braring, I-f: Ilm-free, B: breccia.

Table 4 gives representative chemical compositions of phosphates. Only whitlockites and CFP-phases in the ilm-bearing enclaves contain varying amounts of REE (Ce_2O_3, Nd_2O_3 and Y_2O_3). The concentrations of the other REE were below detection. Figure 1 shows the concentrations of Ce_2O_3 and Y_2O_3. As noted by IKEDA *et al.* (1990), the ratios of Ce_2O_3 and Y_2O_3 are similar, or higher, than that of CI chondrites (ANDERS and GREVESSE, 1989), although those in enclaves 4678 and 4683 are lower. CFP-phases in enclave 4671 are very enriched in Ce_2O_3. The ratios of Ce_2O_3 and Nd_2O_3 are similar to that of CI chondrites (Fig. 2), except for Ce_2O_3-enriched CFP-phases in enclave 4671. Whitlockites in ilm-bearing enclave 4677 are poor in REE.

4.6. Chromite

Chromites occur in all the enclaves studied. Chromites in the ilm-bearing enclaves frequently have (111) lamellae, less than 1 micron in width, as noted by IKEDA *et al.* (1990). RAMDOHR (1973) also described such lamellae of ilmenite in chromite in the Vaca Muerta mesosiderite. Analytical data show that the exsolved phases are ilmenites. We did not find any reduction reaction of oxide minerals as noted by EL GORESY and RAMDOHR (1975) in lunar samples and IKEDA *et al.* (1990).

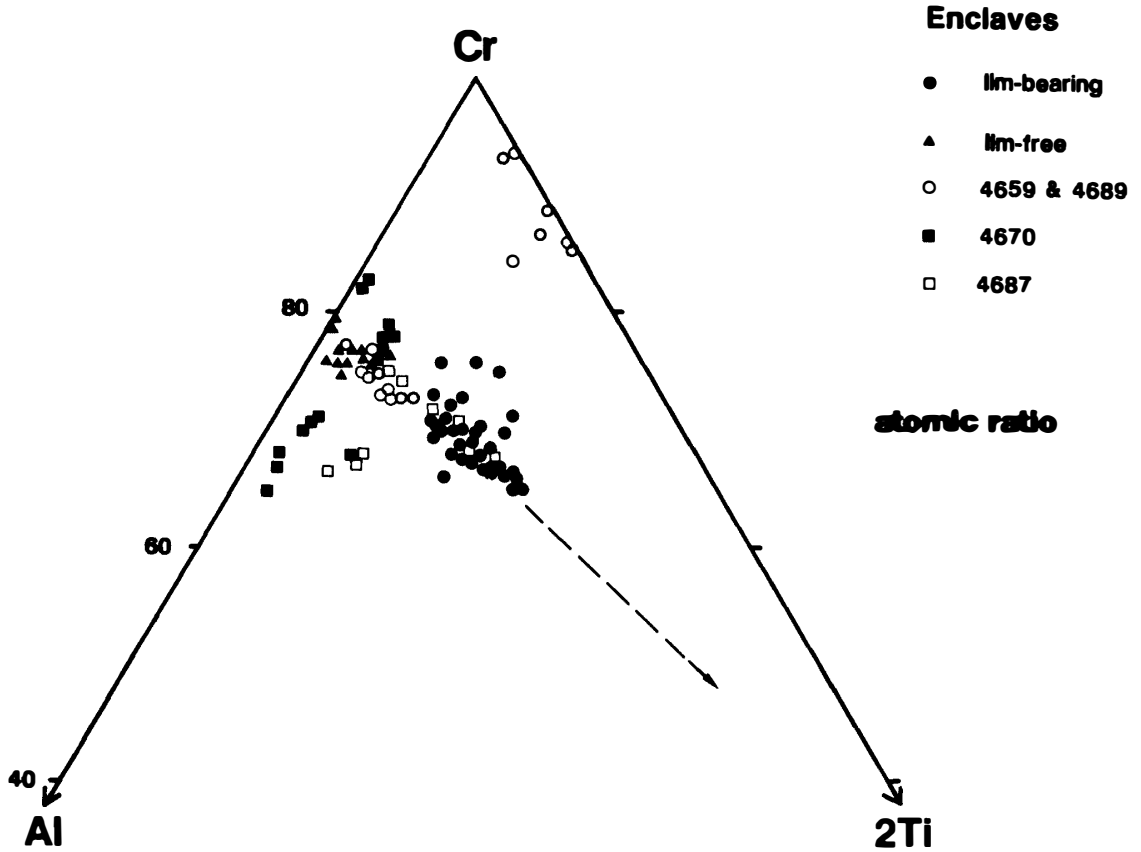

Fig. 3. Compositions of chromites on an atomic Cr-Al-2Ti diagram. 4659 and 4689 are diogenitic enclaves, 4670 is an olivine-orthopyroxenitic enclave, and 4687 a recrystallized breccia. Some chromites in the diogenitic enclaves are depleted in Al. The dashed line is the chemical trend of chromites in the Y-7308 howardite (IKEDA and TAKEDA, 1985).

Table 5 gives representative chemical compositions of chromites, ilmenites and rutiles.

Figure 3 shows the compositions of chromites in all enclaves. Chromites in the ilm-bearing enclaves are more enriched in TiO_2 than those in the ilm-free enclaves. Chromites in diogenitic enclaves have intermediate compositions between these two types of enclaves. Chromites in olivine-orthopyroxenitic enclave 4670 vary widely in Al/Cr ratios. Chromites in a plagioclase-bearing clast are enriched in Al_2O_3. Chromites in orthopyroxene-rich clasts are lower in TiO_2 than those in olivine-rich clasts. Chromites in brecciated enclave 4687 seem to be mixtures between those in all of these enclaves.

We discovered Al_2O_3-free or very depleted chromites from diogenitic enclaves 4659 and 4689 (Fig. 3). These chromites always occur in association with ilmenite and rutile. They typically occur as thin bands like exsolution lamellae in ilmenite (Photo 24). The modal volumes of the chromites are much lower than those of the

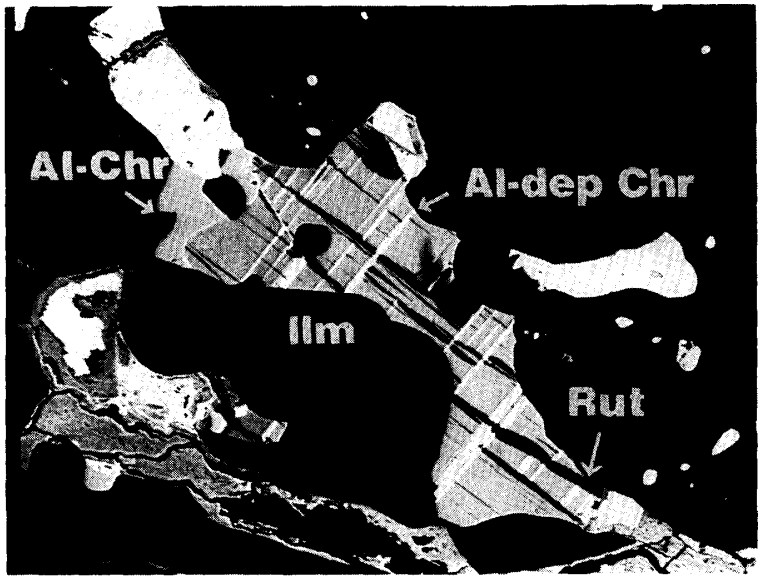

Photo 24. An opaque mineral assemblage consisting of ilmenite (Ilm) with Al_2O_3-bearing (Al-Chr) and Al_2O_3-depleted chromite (Al-dep Chr), and rutile (Rut) in diogenitic enclave 4659. Al_2O_3-depleted chromite and rutile occur as thin bands within ilmenite. BSE image, and width of 200 microns.

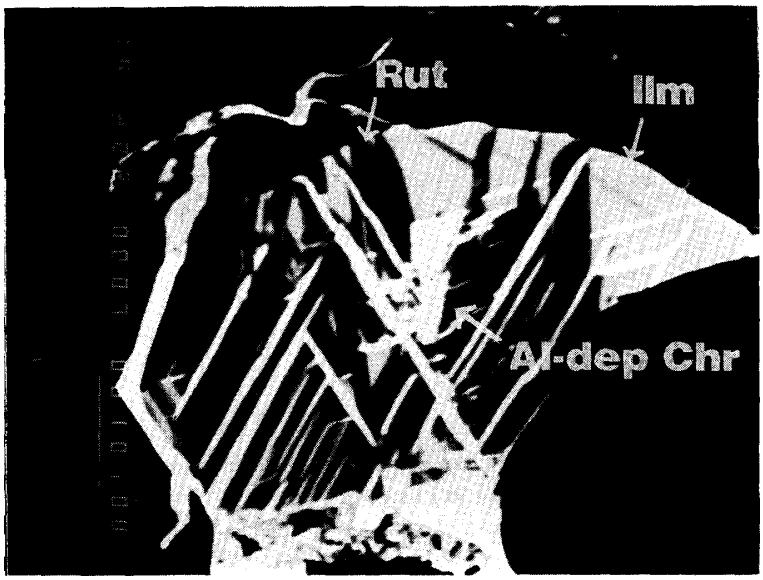

Photo 25. BSE image of an opaque assemblage in diogenitic enclave 4659. It consists of rutile (Rut) and ilmenite (Ilm) with Al_2O_3-depleted chromite veins (Al-dep Chr). Width of 90 microns.

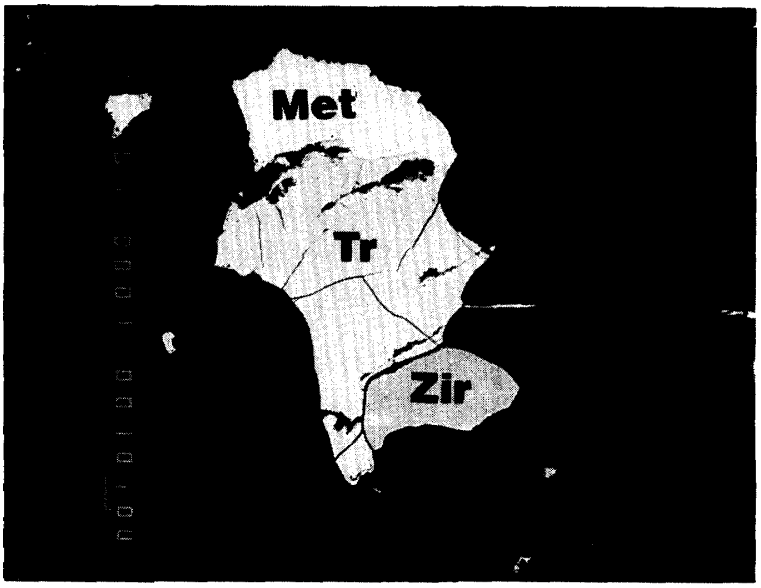

Photo 26. BSE image showing zircon (Zir) with troilite (Tr) and Fe-Ni metal (Met) in brecciated enclave 4687. Width of 200 microns.

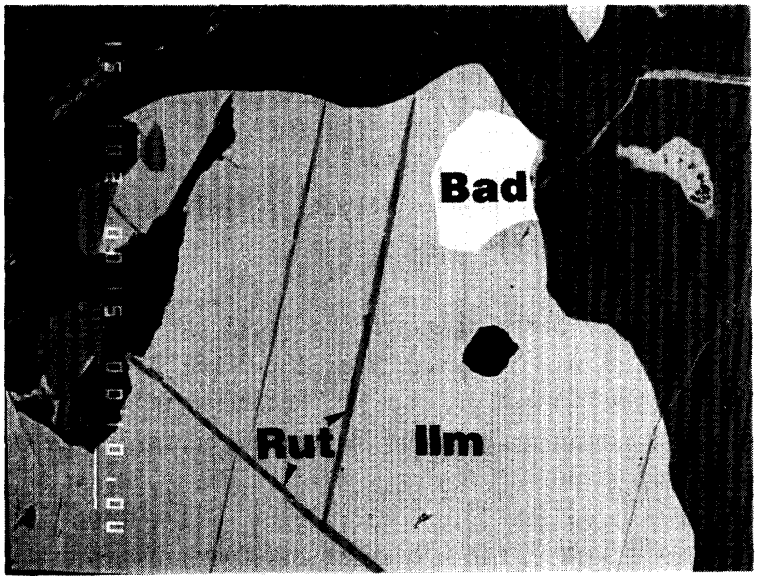

Photo 27. BSE image of baddeleyite (Bad) in ilmenite (Ilm) with rutile (Rut) thin bands in ilm-bearing enclave 4695. Width of 120 microns.

host ilmenites. Rarely, these chromites occur close to normal chromites, although both show no chemical zoning toward one another. The chemistry and occurrence of these Al_2O_3-depleted chromites suggest that they formed by the decomposition of Cr_2O_3-bearing ilmenite or pseudobrookite.

The ZnO contents of chromites are very low (usually below 0.1 wt %), whereas chromites always contain V_2O_3. Al_2O_3-depleted chromites are especially enriched in V_2O_3 (0.7–1.7 wt %) in comparison with other chromites (0.3–1.0 %). The Al_2O_3-depleted chromites are also enriched in MnO (1.3–1.7 % *vs.* 0.4–1.4 % in normal chromites).

4.7. Ilmenite and rutile

Ilmenites and rutiles occur in the ilm-bearing and diogenitic enclaves. Chromites frequently occur in association with ilmenites and/or rutiles. Rutiles always occur

together with ilmenites. Although the volume ratio of rutile and ilmenite in each assemblage varies widely, from nearly equal amounts to very small, thin veins of rutile in ilmenite are the most common occurrences. RAMDOHR (1973) also reported such an intergrowth between rutile and ilmenite in the Vaca Muerta mesosiderite. These occurrences are the result of the decomposition of pre-existing pseudobrookite or exsolution from ilmenite (IKEDA *et al.*, 1990). A grain in diogenitic enclave 4659 consists mainly of rutile and ilmenite with a thin band of Al_2O_3-depleted chromite (Photo 25). This grain may be explained by the decomposition of a Cr_2O_3-bearing pseudobrookite grain.

The MnO contents of ilmenites vary widely from 13.8 to 0.5 wt %, and ilmenites contain more MnO than coexisting chromites. Diogenitic enclaves contain high-MnO ilmenites. These ilmenites also contain 3.0–4.8% MgO, whereas the others have 0.5–2.2%. The other minor element contents are very low (Al_2O_3 <0.05 and Cr_2O_3 <0.5). The concentrations of ZrO_2 in ilmenites are also below detection, although lunar ilmenites contain ZrO_2 up to 0.4% (TAYLOR and MCCALLISTER, 1972). It seems that ZrO_2 is mostly partitioned into zircon or baddeleyite in the Vaca Muerta enclaves.

Although rutiles in some silicates in iron meteorites and a winonaite contain Nb_2O_5 (EL GORESY, 1971; KIMURA, 1990), the concentrations in the enclaves studied here range from 0 to 1.87% and are usually below 0.5 wt %. The host Vaca Muerta mesosiderite also includes Nb_2O_5-poor rutiles (EL GORESY, 1971). Rutiles contain 0.04–2.7% FeO and 0–0.8% Cr_2O_3. The contents of Al_2O_3 and other minor elements are below detection limits.

4.8. Zircon and baddeleyite

Zircon was reported from the Vaca Muerta host mesosiderite (MARVIN and KLEIN, 1964) and from the Mt. Padbury enclave Z (IKEDA *et al.*, 1990). We have found 4 zircon grains, 1 to 30 microns in size, from brecciated enclave 4687. They occur with ilmenite, chromite, troilite and Fe-Ni metal (Photo 26).

We have also found baddeleyite. This mineral is only rarely reported in meteorites. This is the first discovery from mesosiderites. We note that all the ilm-bearing enclaves studied here include several grains of baddeleyite. They typically

Table 6. Representative compositions of zircons (zir) and baddeleyites (bad) in ilm-bearing enclaves (wt %).

Enclave		SiO_2	TiO_2	FeO	HfO_2	ZrO_2	Total
4687	zir	34.47	0.17	0.59	1.38	64.79	101.40
4687	zir	34.38	0.04	0.55	1.00	64.79	100.75
4657	bad	0.00	0.79	0.88	0.55	98.31	100.53
4657	bad	0.00	1.14	1.62	0.91	96.45	100.12
4671	bad	0.00	1.15	1.64	1.31	95.60	99.70
4671	bad	0.24	1.72	2.49	0.50	95.86	100.81
4678	bad	0.00	2.16	1.02	0.88	96.98	101.04
4683	bad	0.43	1.37	2.33	1.60	93.56	99.29
4695	bad	0.00	0.52	0.47	1.74	97.54	100.27
4695	bad	0.00	0.75	1.11	1.90	97.66	101.42

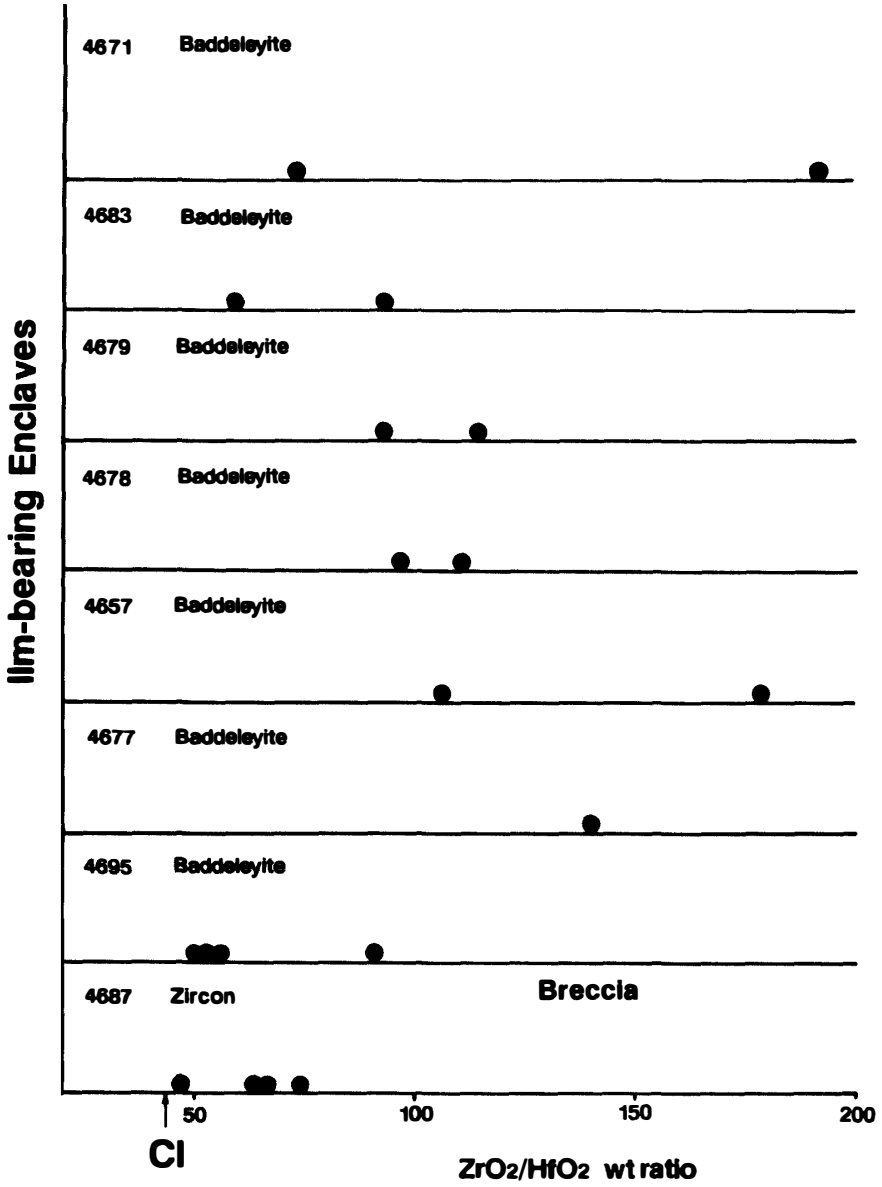

Fig. 4. The ratios of HfO_2 and ZrO_2 wt% of zircons and baddeleyites. Each symbol is for one grain. CI means the CI chondrite ratio of these elements (ANDERS and GREVESSE, 1989).

occur within, or in, the peripheral parts of ilmenite (Photo 27). Their grain size ranges from 1 to 20 microns. They also occur in association with pigeonite, chromite and silica mineral. We did not find any reaction texture between baddeleyite and surrounding phases such as silica mineral. Optical twinning was not observed in baddeleyites, because of their small grain size.

Table 6 gives representative chemical compositions of zircons and baddeleyites from this study. They do not contain any detectable REE. The contents of other minor elements such as Al_2O_3, Cr_2O_3, MnO, MgO, CaO and Nb_2O_5 are below detection. Some baddeleyites appear to include small amounts of TiO_2 and FeO, but they (at least in part) may be the result of overlap with surrounding ilmenites, because the baddeleyites are small and the molar ratios of FeO and TiO_2 are often equal to

that of ilmenite.

The concentrations of HfO_2 were measured in zircons and baddeleyites, and Fig. 4 shows the weight ratios of HfO_2 and ZrO_2. The ZrO_2/HfO_2 ratio is evidently high in most of these grains, compared with that of CI chondrites (ANDERS and GREVESSE, 1989), even if we take into account the experimental error of HfO_2 measurement. However, no mineral is known to prefer HfO_2 to ZrO_2 in enclaves. Thus, it is not yet clear whether HfO_2 was depleted during magmatic fractionation, subsolidus reaction, or condensation from nebular gas.

4.9. Troilite and Fe-Ni metal

Troilite occurs abundantly in brecciated enclaves, whereas it is poor in the ilm-free and ilm-bearing enclaves. Its abundance is always much higher than that of the Fe-Ni metal in enclaves.

The abundance of Fe-Ni metal is extremely low in the ilm-free and ilm-bearing

Table 7. Representative compositions of Fe-Ni metals (wt%).

Sample	Group		Si	P	S	Cr	Fe	Co	Ni	Total
4657	I-b		0.07	0.01		0.02	93.13	0.55	3.46	97.24
4657	I-b		0.06	0.01		0.04	67.16	0.05	31.01	98.32
4671	I-b		0.01	0.00		0.03	55.34	0.00	42.95	98.33
4671	I-b		0.03	0.01		0.07	95.17	0.42	3.25	98.94
4677	I-b		0.04	0.00		0.01	49.42	0.09	49.20	98.75
4677	I-b		0.02	0.02		0.01	93.17	0.60	4.96	98.77
4678	I-b		0.02	0.02		0.01	95.60	0.38	3.58	99.62
4679	I-b		0.04	0.00		0.03	94.74	0.45	3.65	98.91
4679	I-b		0.04	0.01		0.00	82.06	0.28	16.13	98.52
4683	I-b		0.02	0.00		0.02	47.77	0.09	50.37	98.27
4683	I-b		0.03	0.01		0.02	96.19	0.49	3.69	100.44
4695	I-b		0.02	0.00		0.04	94.59	0.46	4.66	99.78
4669	I-f		0.03	0.00		0.06	46.53	0.09	51.67	98.38
4669	I-f		0.05	0.02		0.00	94.35	0.37	4.06	98.85
4672	I-f		0.02	0.00		0.04	77.66	0.21	20.74	98.67
4672	I-f		0.05	0.01		0.11	94.52	0.34	3.67	98.70
4674	I-f		0.04	0.01		0.00	89.24	0.30	9.00	98.59
4659	B	CT	0.03	0.00	0.33	0.02	42.63	0.15	42.81	85.97
4659	B	CT	0.02	0.02	0.29	0.03	47.86	0.13	45.63	93.98
4659	B		0.00	0.00	0.00	0.01	95.10	0.65	4.58	100.34
4659	B		0.00	0.01	0.05	0.00	47.57	0.19	52.71	100.53
4689	B	CT	0.02	0.00	0.13	0.00	45.74	0.05	41.36	87.29
4689	B	CT	0.02	0.00	0.09	0.06	46.96	0.06	43.79	90.97
4689	B		0.01	0.01		0.00	95.55	0.42	4.58	100.57
4689	B		0.02	0.01		0.00	52.88	0.18	47.50	100.59
4670	B	CT	0.01	0.00	0.15		46.50	0.17	35.99	82.82
4670	B	CT	0.01	0.01	0.00		48.54	0.03	41.57	90.16
4670	B		0.02	0.00	0.00		93.42	0.59	5.03	99.06
4670	B		0.03	0.00	0.00		49.05	0.08	50.02	99.18
4687	B		0.00	0.00		0.01	94.09	0.35	4.79	99.24
4687	B		0.02	0.00		0.10	48.05	0.18	50.40	98.75

Group I-b: ilm-bearing, I-f: ilm-free, B: breccia. CT: cloudy taenite.

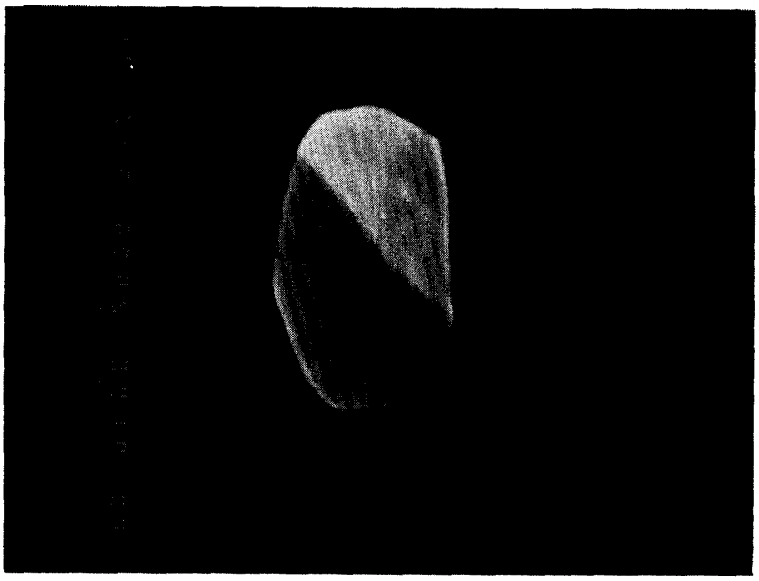

Photo 28. BSE image of a kamacite (dark) and taenite (bright) assemblage in ilm-free enclave 4669. Width of 35 microns.

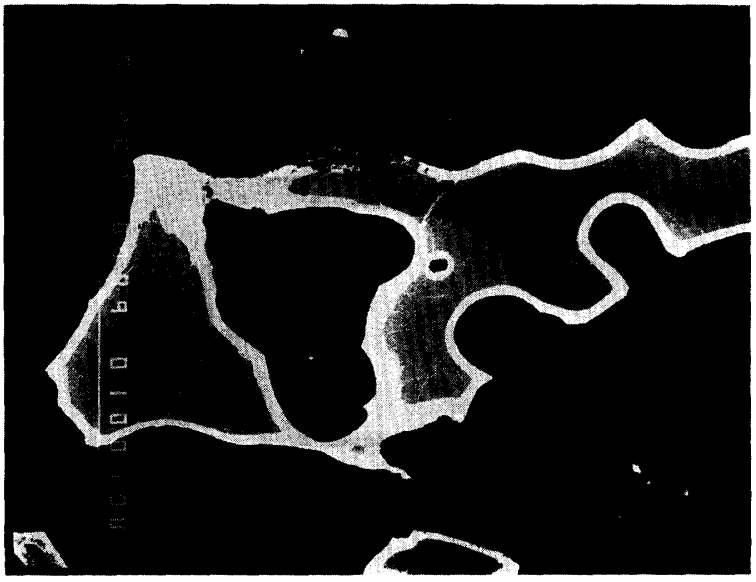

Photo 29. BSE image of cloudy taenite (dark) with a tetra-taenite rim (bright) in olivine-orthopyroxenitic brecciated enclave 4670. The darker part of the cloudy taenite has a low total, and appears to be severely altered. Width of 300 microns.

enclaves. Only brecciated enclaves include abundant metal. Table 7 shows representative compositions of Fe-Ni metal. The Ni and Co contents have no relationship to the occurrence and type of enclave. The concentrations of P, Cr and Si are below detection. Fine-grained Fe-Ni metal frequently consists of kamacite and taenite in all enclaves (Photo 28).

Cloudy taenite occurs in a few brecciated enclaves, and this was also reported in a mesosiderite by AGOSTO *et al.* (1980). It is always rimmed by tetrataenite (or Ni-rich taenite) (Photo 29), with or without kamacite. In comparison with tetra-taenite rims, cloudy taenite is slightly Ni-poor (45.3–40.9 atomic Ni % in enclave 4670, 45.1–50.7 % in enclave 4659, 46.1–48.2% in enclave 4689). The Co contents in both phases are similar. Cloudy taenite usually has low totals (67.6–96.1 wt %). Cloudy taenite often contains S below 0.3 wt %. Sometimes chemical zoning is observed from a tetrataenite rim to Ni-poor cloudy taenite. This structure is con-

sistent with the observations of Fe-Ni metal in iron meteorites and mesosiderites as noted by REUTER *et al.* (1988). According to them, such a structure formed during slow cooling and cloudy taenite is a mixture of Fe_1Ni_1 and martensite with a honeycomb structure. The low total wt % suggests that one of them, perhaps martensite, might have suffered terrestrial alteration. The assemblages of cloudy taenite and tetrataenite also indicate slow cooling (AGOSTO *et al.*, 1980).

5. Bulk Chemistry

5.1. Major elements

Table 8 gives the bulk chemical compositions of the enclaves. Although the petrography of enclaves 4673, 4676, 4681, 4684, 4690 and 4692 is not presented in this paper, the bulk compositions of all of these ilm-bearing enclaves were determined. Enclaves 4630, 4631, 4632, 4633 from Vaca Muerta, and Z, H and U from Mt. Padbury were already described by IKEDA *et al.* (1990).

The bulk chemical compositions characterize the types of enclaves. The content of TiO_2 especially distinguishes the ilm-free and ilm-bearing enclaves (Fig. 5), and is consistent with the presence of TiO_2-oxides and the chemical compositions of the pyroxenes and chromites. The ilm-free enclaves are more magnesian than the ilm-bearing enclaves.

Another intriguing character of the bulk compositional data is the content of

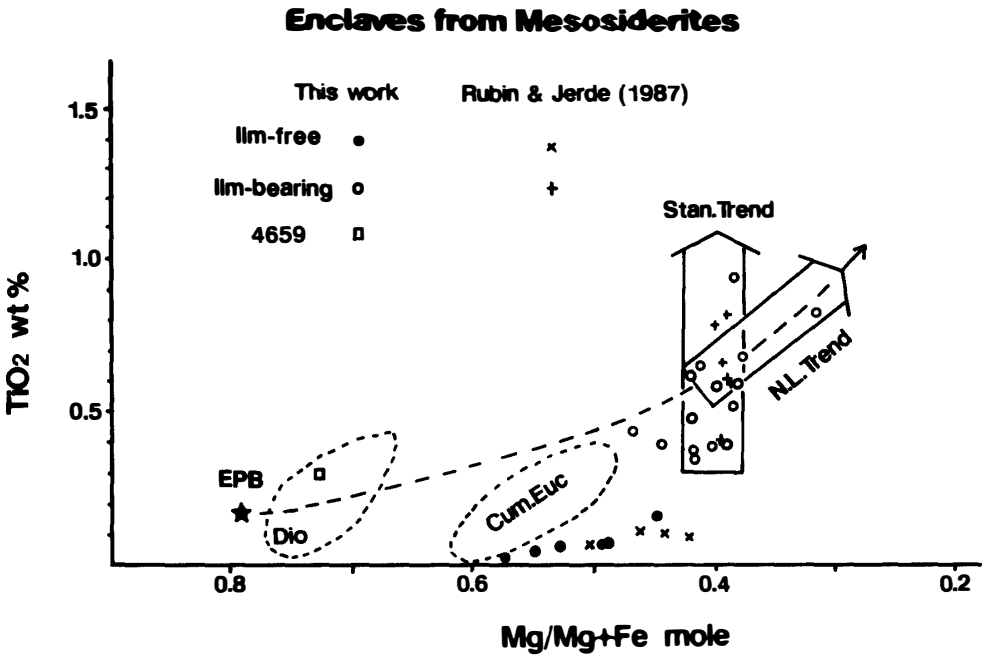

Fig. 5. The atomic Mg/Mg+Fe ratio vs. TiO_2 wt % of the bulk compositions of the enclaves. 4659 is a diogenitic monomict enclave. The Nuevo Laredo (N. L.) and Stannern (Stan.) trends, and the compositional ranges of diogenites and cumulate eucrites are shown in this diagram, after IKEDA (1989). The dashed line shows the fractional crystallization trend from the eucrite parent body composition (EPB, after DREIBUS and WÄNKE, 1980) as calculated by IKEDA (1989).

Table 8. Bulk compositions (wt%) and mg values (atomic Mg/Mg + Fe) of the enclaves. The bulk compositions of silicate and oxide fractions of enclaves 4670 and 4677 were calculated from the modal and mineral compositions. The data of 4659 and 4670-C1 are average compositions of orthopyroxenes.

Enclave	Group	SiO_2	TiO_2	Al_2O_3	Cr_2O_3	FeO	MgO	MgO	CaO	Na_2O	P_2O_5	Total	mg
4631	I-b	50.76	0.64	12.55	0.15	16.80	0.49	6.62	9.95	4.45	0.14	98.56	0.413
4632	I-b	50.33	0.32	12.72	0.07	17.75	0.51	7.15	9.85	0.37	0.14	99.21	0.418
4657	I-b	49.87	0.39	11.99	0.11	18.52	0.63	6.60	9.89	0.41	0.15	98.56	0.388
4671	I-b	49.70	0.55	13.63	0.11	16.73	0.63	6.56	10.08	0.11	0.11	98.54	0.411
4673	I-b	50.00	0.36	12.69	0.11	17.01	0.46	6.89	10.07	0.37	0.17	98.12	0.419
4676	I-b	49.92	0.52	11.78	0.05	18.60	0.44	6.50	9.97	0.38	0.10	98.25	0.384
4677	I-b	51.72	0.73	9.40	0.96	17.34	0.74	8.94	9.00	0.31	0.14	99.29	0.479
4678	I-b	49.38	0.58	12.64	0.30	17.70	0.52	6.02	10.30	0.46	0.22	98.11	0.377
4679	I-b	49.39	0.67	12.08	0.02	18.31	0.52	6.06	10.30	0.45	0.49	98.29	0.371
4681	I-b	49.43	0.39	13.57	0.10	17.35	0.47	7.73	9.89	0.39	0.21	99.52	0.443
4683	I-b	49.23	0.57	12.78	0.11	17.61	0.56	6.53	10.33	0.42	0.18	98.31	0.398
4684	I-b	49.45	0.38	12.43	0.05	18.20	0.50	6.85	10.08	0.37	0.31	98.63	0.402
4690	I-b	47.99	0.40	14.42	0.06	17.68	0.53	6.50	10.30	0.45	0.22	98.55	0.396
4692	I-b	51.30	0.43	12.93	0.22	14.85	0.45	7.23	10.53	0.42	0.65	99.01	0.465
4695	I-b	51.04	0.52	12.66	0.11	17.61	0.59	6.81	9.98	0.43	0.17	99.92	0.408
U	I-b	51.80	0.94	13.66	0.11	15.59	0.50	5.33	11.07	0.41	0.25	99.66	0.379
Z	I-b	51.54	0.82	11.29	0.09	18.73	0.56	4.82	10.11	0.43	0.25	98.64	0.314
4630	I-f	50.70	0.17	13.92	0.13	15.15	0.49	6.76	10.48	0.42	0.39	98.61	0.443
4633	I-f	49.66	0.06	13.67	0.13	15.66	0.55	8.63	9.93	0.30	0.20	98.80	0.496
4669	I-f	49.90	0.07	13.28	0.13	15.64	0.59	8.59	9.82	0.35	0.26	98.61	0.495
4672	I-f	49.09	0.04	14.55	0.14	14.41	0.53	9.94	9.77	0.29	0.32	99.07	0.551
4674	I-f	50.47	0.05	14.59	0.14	13.92	0.49	8.90	10.09	0.33	0.46	99.42	0.533
H	I-f	51.14	0.02	15.08	0.11	12.75	0.50	9.73	9.54	0.20	0.19	99.26	0.576
4659	B	53.27	0.29	0.58	0.47	16.87	0.57	25.31	1.09	0.01		98.46	0.728
4670	B	47.49	0.14	0.69	1.80	17.98	0.60	24.46	0.92	0.02	0.13	99.23	0.746
4670-C1	B	53.73	0.12	0.58	0.41	15.47	0.55	27.51	0.96	0.01		99.34	0.760
4687	B	49.33	0.61	11.19	0.08	18.87	0.52	7.55	9.31	0.41	0.18	98.03	0.416

Group I-b: ilm-bearing, I-f: ilm-free, B: breccia.

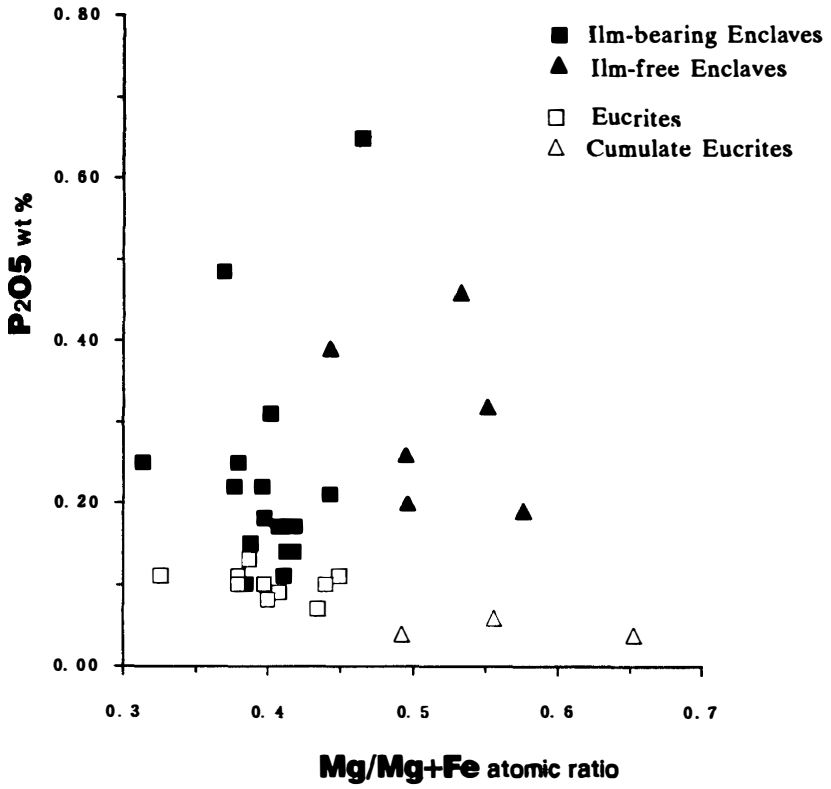

Fig. 6. The atomic Mg/Mg+Fe ratio vs. P_2O_5 wt % of the bulk compositions of the enclaves. The compositions of the eucrites and cumulate eucrites are also plotted (BASALTIC VOLCANISM STUDY PROJECT, 1981).

P_2O_5 (Fig. 6). Non-cumulate eucrites are more enriched in P_2O_5 than magnesian cumulate eucrites. On the contrary, some magnesian ilm-free enclaves are more enriched in P_2O_5 than most of the ilm-bearing enclaves, which is consistent with the common abundance of phosphate in the ilm-free enclaves. This is not to be expected by the crystallization from normal P_2O_5-poor magmas. The ilm-bearing enclaves are also more enriched in P_2O_5 than eucrites.

5.2. Trace elements

Table 9 presents the trace element concentrations of the enclaves studied, as determined by INAA. Except for the brecciated enclaves, the contents of siderophile and chalcophile elements are very low, reflecting the low abundance of Fe-Ni metal and troilite. RUBIN and JERDE (1987) noted that the Ir/Ni ratios of the enclaves are very low. The Ir concentrations of brecciated enclaves 4659 and 4689 are also low, compared with Ni. The Co/Ni, Au/Ni and Ir/Ni weight rations, normalized by the abundances in CI chondrites (ANDERS and GREVESSE, 1989), are 0.161, 0.270 and 0.125 in enclave 4659, and 0.139, 0.261 and 0.129 in enclave 4689, respectively. Thus, Co and Au are also depleted in the enclaves. The depletion of Co reflects the larger amount of taenite or tetrataenite than kamacite. On the other hand, the Co/Ni and Au/Ni ratios in the ilm-free and ilm-bearing enclaves are nearly consistent with those of CI chondrites (ANDERS and GREVESSE, 1989), respectively.

Table 9. Trace element concentrations determined by INAA.

Enclave	Group	Sc ppm	V ppm	Co ppm	Ni ppm	Se ppm	Hf ppm	Ir ppb	Au ppb	La ppm	Ce ppm	Sm ppm	Eu ppm	Yb ppm	Lu pmm
4657	I-b	32.8	85	48.2	1750	1.431	0.621	4.9	19.0	1.26	3.77	0.992	0.449	1.48	0.224
4671	I-b	31.1	105	15.4	365	0.64	1.11	<3.5	10.3	2.20	5.57	1.41	0.507	1.78	0.251
4677	I-b	29.9	83	131	3200	10.81	0.79	<5.8	31.1	2.87	5.15	1.66	0.618	1.96	0.260
4678	I-b	29.1	91	22.3	1700	1.82	0.531	<4.7	17.3	1.16	2.28	0.92	0.587	1.29	0.231
4679	I-b	30.7	79	45.3	1180	1.461	1.30	<5.3	12.3	2.45	4.92	1.40	0.494	1.76	0.270
4683	I-b	34.4	75	56.4	1270	1.70	0.761	<5.2	18.1	0.805	2.09	1.08	0.367	1.64	0.214
4695	I-b	31.4	79	45.6	1040	2.07	1.19	<5.1	12.8	2.89	4.74	1.47	0.595	1.75	0.257
4669	I-f	30.4	86	27.4	685	1.83	<0.13	6.4	20.2	<0.136	<0.56	0.026	0.275	<0.155	<0.028
4672	I-f	24.0	102	42.3	1010	2.67	<0.15	<4.1	13.5	<0.124	<0.87	0.024	0.213	<0.133	<0.0236
4674	I-f	25.6	86	31.9	673	2.08	<0.12	4.6	16.1	<0.133	<0.62	0.044	0.285	<0.148	<0.031
4687	B	28.5	79	120	4580	4.65	1.001	<5.1	27.3	1.88	3.53	1.24	0.543	1.77	0.262
4659	B	10.3	134	115	15700	13.31	<0.26	85.6	53.9	<0.092	<1.23	0.07	<0.116	<0.161	<0.034
4689	B	18.4	179	201	31600	16.9	0.541	178	105	1.67	4.18	1.07	0.305	1.35	0.180

Group I-b: Ilm-bearing, I-f: Ilm-free, B : breccia.

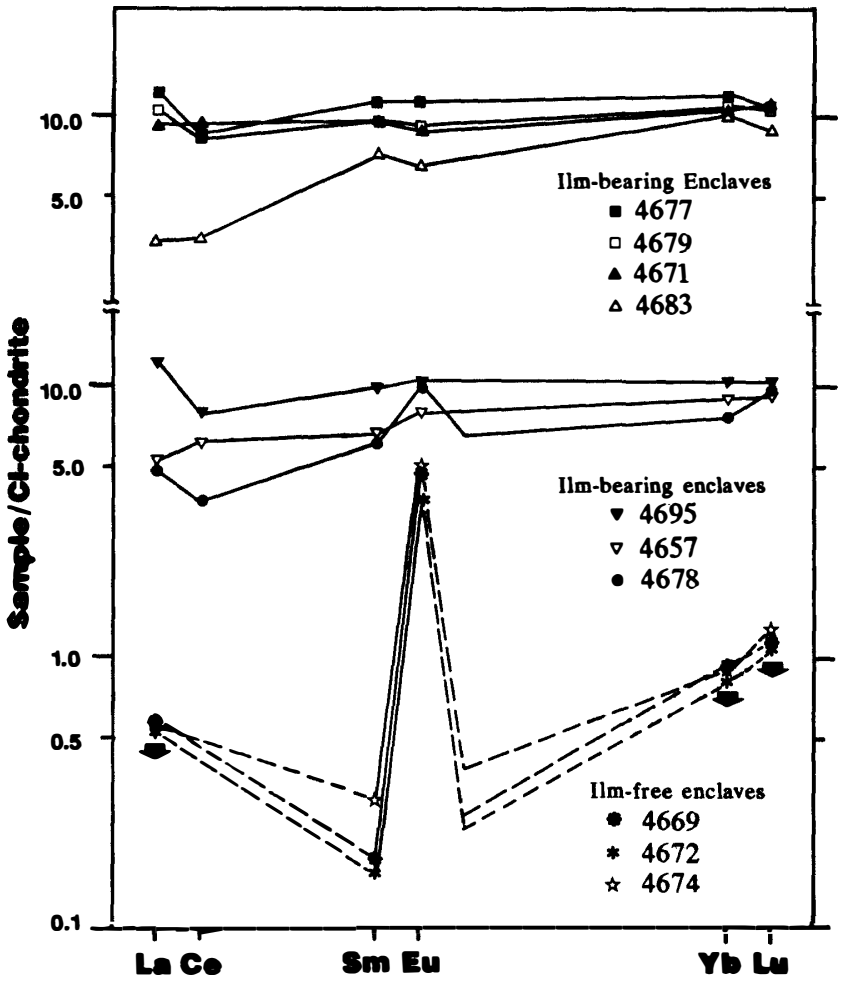

Fig. 7. CI chondrite normalized concentrations of REE in the enclaves. The data of La, Ce, Yb and Lu of the ilm-free enclaves are maximum values, respectively.

Figure 7 shows the CI chondrite normalized concentrations of REE in three ilm-free and seven ilm-bearing enclaves. The Eu/Sm ratios of the ilm-free enclaves are extremely high, consistent with the data of RUBIN and JERDE (1987, 1988), MITTLEFEHLDT (1990) and IKEDA *et al.* (1990). The concentration patterns of REE in the ilm-bearing enclaves are roughly flat. However, there are three kinds of REE patterns for the ilm-bearing enclaves. Enclave 4677 has a flat pattern, and enclaves 4671, 4679 and 4683 seem to have weak negative Eu anomalies, whereas enclave 4678 has a positive Eu anomaly. Enclaves 4657 and 4695 also seem to have a weak positive Eu anomaly.

6. Discussion

6.1. Subsolidus reduction and thermal history of pyroxenes

Pigeonite in most of the ilm-free, and some of the ilm-bearing, enclaves is replaced by orthopyroxene, although the occurrences and abundances differ between these groups. IKEDA *et al.* (1990) concluded that this orthopyroxene formed by subsolidus

reduction from pigeonite, because of the similar CaO contents of both pyroxenes, abundant inclusions of troilite and silica mineral in orthopyroxene, and the extension of augite lamellae into orthopyroxene from pigeonite. They suggested the following reduction equation:

$$\underset{\text{Fs}}{FeSiO_3} + \underset{\text{Gas}}{H_2S} \rightarrow \underset{\text{Tr}}{FeS} + \underset{\text{Sil}}{SiO_2} + \underset{\text{Gas}}{H_2O}, \quad (1)$$

where Fs, Tr, and Sil are ferrosilite component in pigeonite, troilite and silica mineral, respectively.

Our observations of orthopyroxene and pigeonite in this study support the idea of subsolidus reduction replacement. The observation that orthopyroxene surrounds pigeonite (Photos 2 and 4) is not consistent with a terrestrial magmatic crystallization sequence. Photos 22 and 23 show that the abundant troilite and silica mineral grains occur in orthopyroxene, not in pigeonite, and this supports the proposed reduction reaction (1). We found a slight enrichment of CaO in orthopyroxene compared with coexisting pigeonite, and this observation is also contrary to the origin of orthopyroxene by igneous processes or normal inversion from pigeonite. Alternatively, it is probable that orthopyroxene became enriched in CaO through the reduction reaction (1). As suggested by IKEDA *et al.* (1990), the extension of thick augite lamellae from pigeonite to orthopyroxene is a strong textural support that this reduction occurred under subsolidus conditions, and not during the magmatic stage.

In the ilm-free enclaves, tiny grains of whitlockite occur cutting the thick augite lamellae in orthopyroxene (Photo 22). These whitlockites do not occur in pigeonite, and frequently coexist with silica mineral and troilite. Such an occurrence of whitlockite suggests the following reaction modified from the original equation by AGOSTO *et al.* (1980):

$$\underset{\text{Wo}}{3CaSiO_3} + \underset{\text{Fs}}{5FeSiO_3} + \underset{\text{Gas}}{2P} + \underset{\text{Gas}}{5H_2S} \rightarrow \underset{\text{Whi}}{Ca_3(PO_4)_2} + \underset{\text{Tr}}{5FeS} + \underset{\text{Sil}}{8SiO_2} + \underset{\text{Gas}}{5H_2}, \quad (2)$$

where Wo, Fs, Whi, Tr and Sil are wollastonite component, ferrosilite component, whitlockite, troilite and silica mineral, respectively. The source of phosphorus is not yet clear. The concentrations of REE in these whitlockites are below detection limits, which is consistent with the above reaction. HARLOW *et al.* (1982) also suggested that most of the phosphates in mesosiderites did not form by igneous fractionation, but by a different reduction reaction between pyroxene and P-bearing metal. They criticized the reduction reaction proposed by AGOSTO *et al.* (1980), because of the absence of a close correlation of silica mineral and phosphate abundance. We observed that silica mineral is much more abundant than phosphate in reduced orthopyroxenes. Although it is difficult to evaluate which silica mineral formed by reaction (1) or (2), our observations do not disagree with reaction (2). Whitlockites are common in the orthopyroxene of the ilm-free enclaves. The ilm-free enclaves are more enriched in P_2O_5 than cumulate eucrites and ilm-bearing enclaves, which is consistent with the high abundance of these whitlockites. NEHRU *et al.* (1980a) also found that gabbroic clasts are more enriched in tridymite and phosphate than

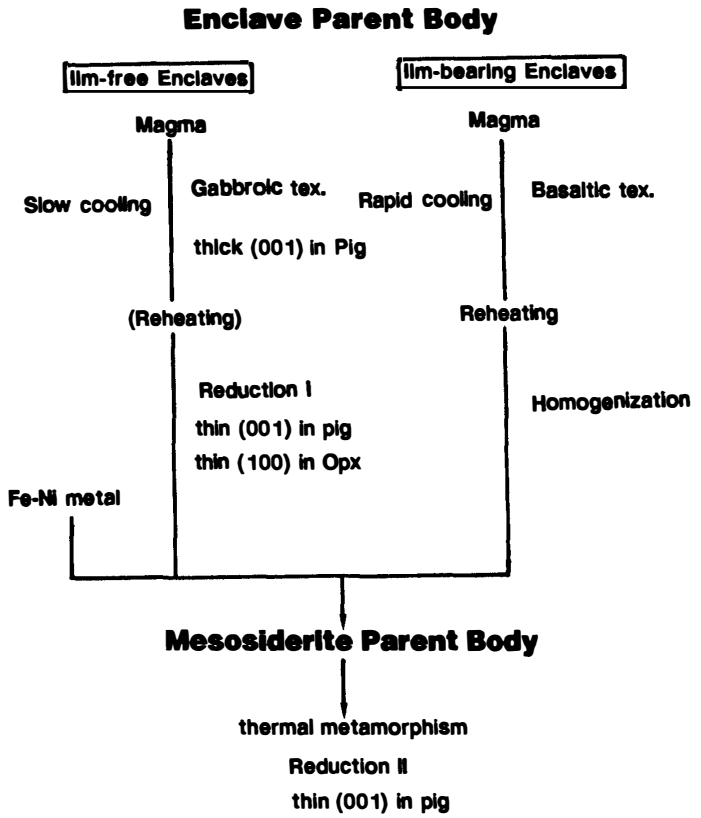

Fig. 8. A schematic diagram showing the thermal history of the enclaves and their pyroxenes. Pig and Opx are pigeonite and orthopyroxene, respectively. Note that reduction (1) took place in an enclave parent body prior to the formation of mesosiderite parent body, whereas reduction (2) after the mesosiderite formation.

basaltic clasts in mesosiderites. The abundant orthopyroxene and whitlockite of reduction origin suggest that the ilm-free enclaves were more reduced than the ilm-bearing enclaves.

Now we consider the thermal histories of the pyroxenes and enclaves from the observations made in this study (Fig. 8). Gabbroic textures suggest slow cooling, whereas ophitic textures indicate rapid cooling from magma. In spite of the variety of textures, the constituent minerals are homogeneous in most of the enclaves. Such homogeneity of the constituent minerals requires reheating and probably slow cooling, especially for the ilm-bearing enclaves.

Subsolidus reduction occurred after homogenization of the enclaves, because slight zoning is encountered only in pigeonite and orthopyroxene pairs in enclaves. Reduction occurred after the exsolution of thick augite in the ilm-free enclaves. Pigeonite and orthopyroxene include further thin augite lamellae of (001) and (100) directions, respectively. They exsolved after reduction. On the other hand, thick lamellae of augite do not occur in the ilm-bearing enclaves. Instead, orthopyroxene in them contains augite blebs which seem to be decomposition products from calcic pigeonite. It is possible that the original calcic pigeonite was reduced and decomposed to form the orthopyroxene and augite blebs. After reduction, thin lamellae of augite exsolved from pigeonite.

Only the ilm-free enclaves were extensively reduced, which suggests that this reduction occurred before the mixing with Fe-Ni metal in the mesosiderite parent body. Otherwise, the ilm-bearing enclaves would have been also extensively reduced as are the ilm-free enclaves. The reduction of the ilm-free enclaves might have occurred in a deeper portion of the enclave parent body (IKEDA *et al.*, 1990). On the other hand, orthopyroxene occurs only in the peripheral parts of several ilm-bearing enclaves. Accordingly, it is probable that this reduction occurred after the mixing with Fe-Ni metal in the mesosiderite parent body. Thus, we can distinguish between two stages of subsolidus reduction, *i.e.*, reduction (I) before the mixing with metal, and reduction (II) after the mixing with metal, which is probably the well known reduction in host mesosiderites.

AGOSTO *et al.* (1980) and others have argued that the SiO_2-enriched bulk compositions of mesosiderites can be explained by *in situ* reduction. Although ilm-free enclave 4674 is enriched in P_2O_5 (0.46 wt%), this amount of phosphorus cannot explain the enrichment of the silica mineral at all. Enclave 4674 contains only 0.4 wt% troilite, and Fe-Ni metal is present only in trace amounts. Therefore, subsolidus *in situ* reduction cannot explain the enrichment of the silica minerals, at least for the enclaves.

Brecciated enclaves always include a large amount of troilite. This is especially so for diogenitic brecciated enclave 4659 which has about 10 vol% troilite. However, it is unlikely that this troilite formed through a reduction reaction, because the enclave does not contain any silica mineral. Alternatively, troilite may have been mechanically introduced during brecciation. Troilite is abundantly distributed in the interstices between fine to coarse orthopyroxene fragments or clasts in enclave 4659. The abundance of troilite is always much higher than that of Fe-Ni metal in the enclaves. This is different from the host mesosiderites. The sulfur fugacity might have been much higher than that in the mesosiderite parent body.

6.2. *Magmatic crystallization of the enclaves*

Figure 5 shows the atomic Mg/Mg+Fe ratio (mg value) *vs.* TiO_2. Diogenitic enclave 4659 falls in the region of diogenites. The ilm-free enclaves are very depleted in TiO_2 and fall below the region of cumulate eucrites. Most of the ilm-bearing enclaves fall in the region of the Stannern trend which is regarded as the partial melting trend (WARREN and JERDE, 1987), although some of them overlap the Nuevo Laredo trend. Enclave Z, from Mt. Padbury, is within the Nuevo Laredo trend which is the fractional crystallization trend of the predominant eucrites. One ilm-bearing enclave 4692 is evidently out of the region of both trends. This enclave is more enriched in MgO and P_2O_5 than are the other ilm-bearing enclaves. Replacement textures of orthopyroxene are well-developed in the marginal parts. This enclave might have suffered severe secondary reduction.

Eucrites of the Stannern trend are less abundant than those of the Nuevo Laredo, whereas enclaves of the Stannern trend are much more abundant. This is a point of difference between the two meteorite groups, although this may be due to a sampling problem.

It is probable that most of the ilm-bearing enclaves formed from a magma of

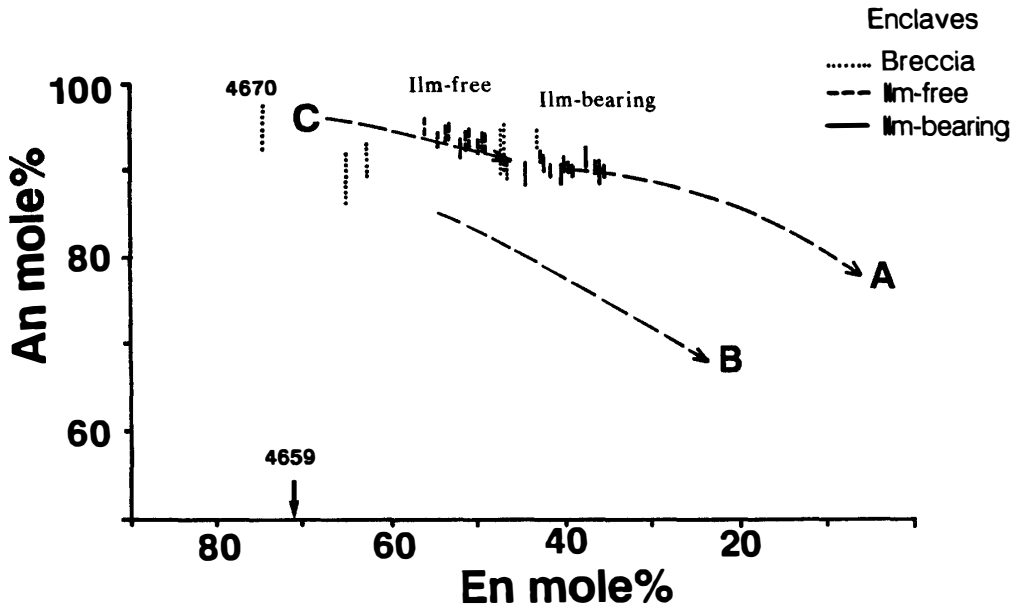

Fig. 9. Anorthite mole % plagioclase vs. enstatite mole % major pyroxene (orthopyroxene from diogenitic and olivine-orthopyroxenitic enclaves; pigeonites from the others). Trends A, B and C are the alkali-poor, alkali-rich and cumulate-eucrite trends of the HED meteorites, respectively (IKEDA and TAKEDA, 1985). A diogenitic breccia 4659 does not include any plagioclase. 4670 is an olivine-orthopyroxenitic monomict breccia.

partial melting origin, since they fall within the Stannern trend. The occurrence of baddeleyite is consistent with the partial melting origin, because Zr is a highly incompatible element. Baddeleyite has not yet been repoted from the HED meteorites. Only SAIKI and TAKEDA (1990) reported one grain of a baddeleyite-like phase from the polymict eucrite Y-75011. Zircons occur in enclaves 4687 and Z. Enclave 4687 is a breccia and zircon occurs with troilite and other phases as fragments. Although the bulk mg value of enclave 4687 is higher than that of the ilm-bearing enclaves, zircon might have come from a fraction similar to enclave Z. Zircon is only rarely encountered in HED meteorites. It occurs only in the Bouvante eucrite (CHRISTOPHE MICHEL-LEVY *et al.*, 1980), Malvern howardite (DESNOYERS and JEROME, 1977) and unique eucrite Y-791438 (SAIKI and TAKEDA, 1990). Thus, the ZrO_2-concentrations of the enclave and the eucrite magmas may have been different.

The anorthite mole % of plagioclase *vs.* the average enstatite mole % of the main pyroxene in each enclave is shown in Fig. 9. The ilm-free enclaves follow trend C of the cumulate eucrites by IKEDA and TAKEDA (1985), although the ilm-free enclaves are more enriched in anorthite component. The ilm-bearing enclaves follow trend A which is the crystallization trend in the magma ocean of the eucrite parent body. If most of the ilm-bearing enclaves formed by partial melting, they should follow trend B of the eucrites which is the partial melting trend. Therefore, it is probable that the parental magmas of the ilm-bearing enclaves were more depleted in Na_2O than those of the eucrites. The bulk content of Na_2O in the ilm-bearing enclaves ranges from 0.31 to 0.45 wt%, whereas that in the eucrites from 0.45 to 0.60 wt% (BASALTIC VOLCANISM STUDY PROJECT, 1981).

Figure 10 is an oxygen plot of the bulk compositions of the enclaves onto the

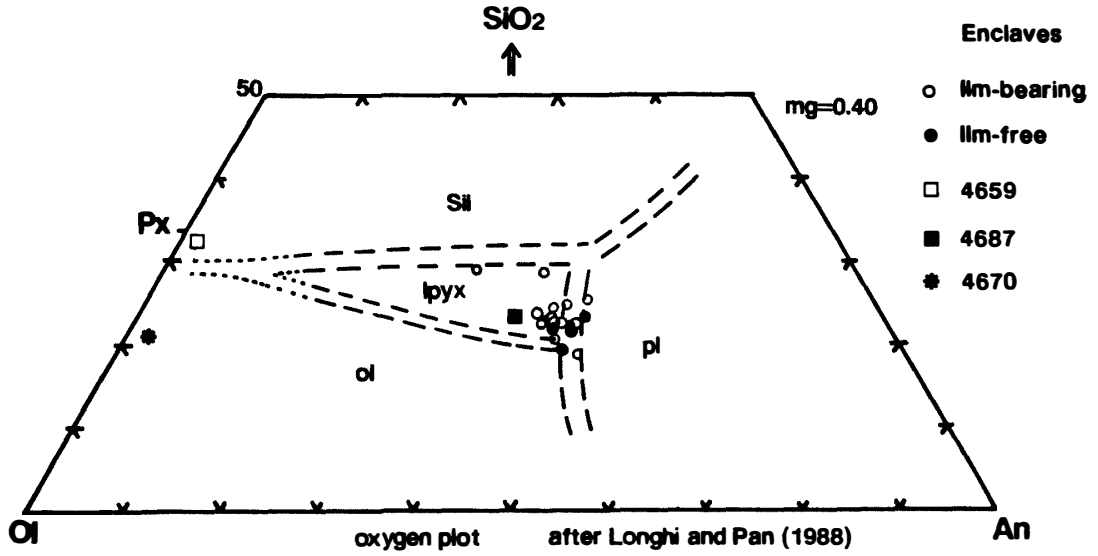

Fig. 10. An oxygen plot of the enclaves in a ternary diagram of silica, olivine and anorthite, with a 0.40 mg value (after LONGHI *and* PAN*, 1988). The liquidus fields of silica mineral (sil), olivine (ol), low-Ca pyroxene (lpyx) and plagioclase (pl), and the liquidus bondaries between them are shown. 4659 is a diogenitic enclave, 4687 a recrystallized brecciated enclave, and 4670 an olivine-orthopyroxenitic enclave.*

SiO_2–olivine–anorthite diagram of LONGHI and PAN (1988). Most of the enclaves fall near the eutectic point or the boundary between the pyroxene and plagioclase fields, which is consistent with a partial melting origin for these enclaves. One breccia (enclave 4687) has an intermediate composition, between the ilm-bearing and diogenitic enclaves. This is consistent with its brecciated texture and mineralogy. Two enclaves, 4677 and Z, fall on the liquidus boundary between the pyroxene and silica mineral fields. Enclave 4677 is especially depleted in plagioclase component, and such a depletion cannot be explained by reduction or oxidization during the subsolidus or magmatic stage, from a magma of partial melting origin. Alternatively, they probably formed through fractional crystallization from another magma, and this is consistent with enclave Z being on the Nuevo Laredo trend (Fig. 5). The abundant silica minerals in enclave 4677 show euhedral to subhedral forms against plagioclase, and this is consistent with primary crystallization of the silica minerals. We present below a model for the origin of such SiO_2-rich magmas. If a primary ultramafic magma was fractionated by the crystallization of olivine, and the liquid then entered the pyroxene liquidus field, it could become magnesian enough to produce a SiO_2-enriched residual magma by the separation of pyroxene.

Figure 11 shows the mole plot of the enclaves onto a ternary diagram of silica, olivine and anorthite. Most of the enclaves fall within or near the region of non-cumulate eucrites, although some are more enriched in anorthite component than eucrites. As noted by IKEDA *et al.* (1990), the ilm-free enclaves are much more enriched in silica mineral component than cumulate eucrites. It is well known that the silicate fractions of mesosiderites are more SiO_2-enriched than the howardites (PRINZ *et al.*, 1980). However, subsolidus reduction with Fe-Ni metal cannot explain both

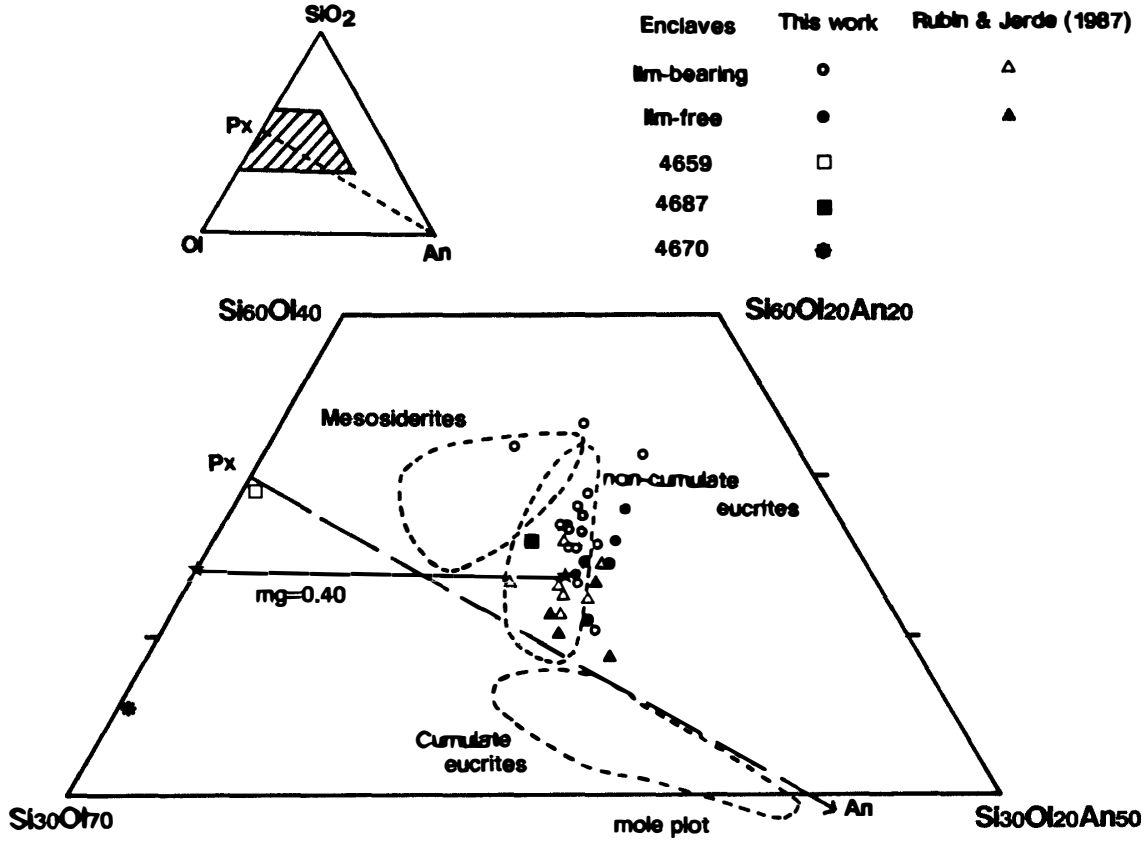

Fig. 11. Mole ratios, of olivine (Ol), anorthite (An) and silica (Si), of the bulk compositions of the enclaves (after STOLPER, *1977). The compositional ranges of the non-cumulate and cumulate eucrites, and mesosiderites, are shown (after* MASON *et al., 1979;* MITTLEFEHLDT *et al., 1979). The straight line is the assumed boundary between the olivine and pyroxene liquidus fields for a eucritic magma with a 0.40 mg value (*IKEDA *and* TAKEDA, *1985). The solid star is the peritectic point (*STOLPER, *1977). 4659 is a diogenitic enclave, 4687 a recrystallized brecciated enclave, and 4670 an olivine-orthopyroxenitic enclave.*

the SiO_2-enrichment and the petrography of the enclaves, as noted before. Accordingly, our discovery of highly SiO_2-enriched enclaves is an important key in explaining the enrichment of SiO_2. We propose that the silicate fractions of mesosiderites are mixtures of diogenitic rocks (*e. g.*, enclave 4659), ilm-free and ilm-bearing, and SiO_2-enriched components. Secondary reduction in the mesosiderite parent body resulted in further SiO_2-enrichment.

6.3. REE and the history of enclaves

The wide variation of REE contents in whitlockites were first reported by IKEDA *et al.* (1990), and they suggested that this variation is related to terrestrial alteration. The REE contents of whitlockites obtained here also vary widely. This can be explained either by (a) primary variation during crystallization, or by (b) terrestrial alteration. In the case of (a), the depletion of Y_2O_3, compared with Ce_2O_3 and Nd_2O_3, may be due to difference in the partitioning of these elements into whitlockite and other phases, depending on temperature. For example, pyroxene may prefer Y_2O_3

to Ce_2O_3 and Nd_2O_3. Alternatively, the primary magma of the enclaves may have been depleted in Y_2O_3 for unknown reasons. In the case of (b), Y_2O_3 could be lost easily from whitlockite under terrestrial conditions.

The extraordinarily high ratios of Eu/Sm in the ilm-free enclaves obtained here are consistent with the idea that the ilm-free (gabbroic) enclaves were derived from repeatedly partially-melted cumulate gabbros (RUBIN and JERDE, 1988). Some ilm-bearing enclaves show positive and others negative Eu anomalies, and this may be the result of plagioclase-enriched or pigeonite-enriched source materials, through partial melting.

6.4. Comparison with HED meteorites

We summarize the differences between the HED meteorites and the enclaves, based on the observations obtained here, as follows;

(1) The Na_2O-contents in the ilm-free and ilm-bearing enclaves are depleted when compared with those of the eucrites.

(2) The P_2O_5-contents of the enclaves are enriched, when compared with the eucrites. Some ilm-free enclaves are especially enriched in P_2O_5, and this can be explained by subsolidus reduction and the secondary formation of whitlockite.

(3) Pigeonites were probably reduced under subsolidus conditions, especially in the ilm-free enclaves. Such reduction has not been observed in the HED meteorites.

(4) The common occurrence of ZrO_2-bearing phases characterizes the ilm-bearing enclaves. These phases have only rarely been reported in the HED meteorites.

(5) The bulk compositions of the enclaves are generally more SiO_2-enriched than those of the HED meteorites. This is not due to secondary reduction with Fe-Ni metal in those large enclaves, but mainly due to the presence of moderately to highly SiO_2-enriched materials. Highly SiO_2-enriched rocks or clasts have not been observed in the HED meteorites.

These characteristic features of the enclaves originated before the mixing with Fe-Ni metal in the mesosiderite parent body. They are primary features of the enclaves which formed in the enclave parent body. Accordingly, it is probable that the enclave parent body and its magmas were different from those of the HED meteorites. However, we cannot exclude the possibility that both came from a common parent body which was very heterogeneous in structure and composition.

7. Conclusions

(1) Thirty-eight enclaves from the Vaca Muerta mesosiderite were studied, and fourteen were especially studied by SEM-petrography. These enclaves are classified into the ilm-free, ilm-bearing and breccia groups. We have discovered an olivine-orthopyroxenite and two diogenitic brecciated enclaves.

(2) Pigeonite in the ilm-free enclaves was frequently replaced by orthopyroxene along with troilite, silica mineral and whitlockite, by subsolidus reduction. This reduction occurred before the mixing with Fe-Ni metal on the mesosiderite parent body. On the other hand, such reduction occurred only sparsely in the ilm-bearing enclaves, and it occurred after the Fe-Ni metal was mixed on the mesosiderite parent

body. Thus, two stages of subsolidus reduction occurred in the enclaves.

(3) Various subsolidus reaction textures of chromite, ilmenite, rutile, and probably pre-existing pseudobrookite, were found. Al_2O_3-depleted chromite formed through the decomposition of ilmenite and pseudobrookite.

(4) We found two kinds of ZrO_2-bearing minerals, zircon and baddeleyite. The latter is the first discovery in mesosiderites. The ilm-bearing enclaves always include baddeleyite. A depletion of HfO_2, compared with ZrO_2, is commonly observed, although the reason for this is not yet clear.

(5) The bulk compositions of the enclaves were measured, and they are SiO_2-enriched, when compared with the HED meteorites. This is especially so for the highly SiO_2-enriched ilm-bearing enclaves. They probably formed by fractional crystallization, whereas the other ilm-bearing enclaves formed through partial melting. The SiO_2 enrichment of the silicate portion of the mesosiderites can be explained as being mainly due to the mixing of enclaves of partial melting origin, highly SiO_2-enriched enclaves, and diogenitic enclaves rather than *in situ* reduction being the major process.

(6) All of these differences, between the enclaves and the HED meteorites, strongly suggest that the parent bodies of both meteorites were different from one another.

Acknowledgments

We are indebted to the reactor comittee of the University of Tokyo for the reactor facility of Rikkyo University. This work was supported by NASA grant NAG 9–32 (M. PRINZ, P. I.)

References

AGOSTO, W. N., HEWINS, R. H. and CLARKE, R. S., JR. (1980): Allan Hills A77219, the first Antarctic mesosiderites. Proc. Lunar Planet. Sci. Conf., 11th, 1027–1045.

ANDERS, E. and GREVESSE, N. (1989): Abundances of the elements: Meteoritic and solar. Geochim. Cosmochim. Acta, **53**, 197–214.

BASALTIC VOLCANISM STUDY PROJECT (1981): Basaltic Volcanism on the Terrestrial Planets. New York, Pergamon Press, 1286 p.

CHRISTOPHE MICHEL-LEVY, M., JEROME, D. Y., PALME, H., SPETTEL, B. and WÄNKE, H. (1980): The Bouvante eucrite. Meteoritics, **15**, 272–273.

DELANEY, J. S., NEHRU, C. E. and PRINZ, M. (1980): Olivine clasts from mesosiderites and howardites: Clues to the nature of achondritic parent bodies. Proc. Lunar Planet. Sci. Conf., 11th, 1073–1087.

DELANEY, J. S., NEHRU, C. E., PRINZ, M. and HARLOW, G. E. (1981): Metamorphism in mesosiderites. Proc. Lunar Planet. Sci. Conf., 12th, 1315–1342.

DELANEY, J. S., HARLOW, G. E., NEHRU, C. E., O'NEILL, C. and PRINZ, M. (1982): Mount Padbury mafic "Enclaves" and the petrogenesis of mesosiderite silicates. Lunar Planet. Sci. **XIII**. Houston, Lunar Planet. Inst., 152–153.

DELANEY, J. S., TAKEDA, H., PRINZ, M., NEHRU, C. E. and HARLOW, G. E. (1983): The nomenclature of polymict basaltic achondrites. Meteoritics, **18**, 103–111.

DESNOYERS, C. and JEROME, D. Y. (1977): The Malvern howardite: A petrological and chemical discussion. Geochim. Cosmochim. Acta, **41**, 81–86.

DREIBUS, G. and WÄNKE, H. (1980): The bulk composition of the eucrite parent asteroid and its bearing on planetary evolution. Z. Naturforsch., **35a**, 204–216.

EL GORESY, A. (1971): Meteoritic rutile: A niobium-bearing mineral. Earth Planet. Sci. Lett., **11**, 359–361.

EL GORESY, A. and RAMDOHR, P. (1975): Subsolidus reduction of lunar opaque oxides: Textures, assemblages, geochemistry, and evidence for a late-stage endogenic gaseous mixture. Proc. Lunar Sci. Conf., 6th, 729–745.

FLORAN, R. J. (1978): Silicate petrography, classification, and origin of the mesosiderites: Review and new observations. Proc. Lunar Planet. Sci. Conf., 9th, 1053–1081.

HARLOW, G. E., DELANEY, J. S., NEHRU, C. E. and PRINZ, M. (1982): Metamorphic reactions in mesosiderites: Origin of abundant phosphate and silica. Geochim. Cosmochim. Acta, **46**, 339–348.

HEWINS, R. H. (1979): The pyroxene chemistry of four mesosiderites. Proc. Lunar Planet. Sci. Conf., 10th, 1109–1125.

IKEDA, Y. (1989): Igneous activity in early solar system based on HED and mesosiderite meteorites. Abs. IGC 28th, 2-92–2-93.

IKEDA, Y. and TAKEDA, H. (1985): A model for the origin of basaltic achondrites based on the Yamato-7308 howardite. Proc. Lunar Planet. Sci. Conf., 15th, Pt. 2, C649–C663 (J. Geophys. Res., **90** Suppl.).

IKEDA, Y., EBIHARA, M. and PRINZ, M. (1990): Enclaves in the Mt. Padbury and Vaca Muerta mesosiderites: Magmatic and residue (or cumulate) rock types. Proc. NIPR Symp. Antarct. Meteorites, **3**, 99–131.

KIMURA, M. (1990): Antarctic two new winonaites, Y-74025 and Y-75305: Mineralogy and classification. Papers Presented to the 15th Symposium on Antarctic Meteorites, May 30–June 1, 1990. Tokyo, Natl Inst. Polar Res., 191.

LONGHI, J. and PAN, V. (1988): A reconaissance study of phase boundaries in low-alkali basaltic liquids. J. Petrol., **29**, 115–147.

MARVIN, U. B. and KLEIN, C. (1964): Meteoritic zircon. Science, **146**, 919–920.

MASON, B., JAROSEWICH, E. and NELEN, J. A. (1979): The pyroxene-plagioclase achondrites. Smithson. Contrib. Earth Sci., **22**., 27–45.

MCCALL, G. J. H. (1966): The petrology of the Mount Padbury mesosiderite and its achondrite enclaves. Mineral. Mag., **35**, 1029–1060.

MITTLEFEHLDT, D. W. (1979): Petrographic and chemical characterization of igneous lithic clasts from mesosiderites and howardites and comparison with eucrites and diogenites. Geochim. Cosmochim. Acta, **43**, 1917–1935.

MITTLEFEHLDT, D. W. (1990): Petrogenesis of mesosiderites: I. Origin of mafic lithologies and comparison with basaltic achondrites. Geochim. Cosmochim. Acta, **54**, 1165–1173.

MITTLEFEHLDT, D. W., CHOU, C. L. and WASSON, J. T. (1979): Mesosiderites and howardites: Igneous formation and possible genetic relationships. Geochim. Cosmochim. Acta, **43**, 673–688.

NEHRU, C. E., HARLOW, G. E., PRINZ, M. and HEWINS, R. H. (1978): The tridymite-phosphate-rich component in mesosiderites. Meteoritics, **13**, 573.

NEHRU, C. E., PRINZ, M., DELANEY, J. S., HARLOW, G. E. and FRISHMAN, S. (1980a): Gabbroic and basaltic clasts in mesosiderites: Unique achondritic tridymite-phosphate-rich, two-pyroxene rock types. Lunar Planet. Sci. **XI**. Houston, Lunar Planet Inst., 803–805.

NEHRU, C. E., ZUCKER, S. M., HARLOW, G. E. and PRINZ, M. (1980b): Olivines and olivine coronas in mesosiderites. Geochim. Cosmochim. Acta, **44**, 1103–1117.

POWELL, B. N. (1971): Petrology and chemistry of mesosiderites- II. Silicate textures and compositions and metal-silicate relationships. Geochim. Cosmochim. Acta, **35**, 5–34.

PRINZ, M., NEHRU, C. E., DELANEY, J. S., HARLOW, G. E. and BEDELL, R. L. (1980): Modal studies of mesosiderites and related achondrites, including the new mesosiderite ALHA 77219. Proc. Lunar Planet. Sci., 11th, 1055–1071.

RAMDOHR, P. (1973): The Opaque Minerals in Stony Meteorites. Elsevier, Amsterdam, 245 p.

REUTER, K. B., WILLIAMS, D. B. and GOLDSTEIN, J. I. (1988): Low temperature phase transformations

in the metallic phases of iron and stony-iron meteorites. Geochim. Cosmochim. Acta, **52**, 617–626.

RUBIN, A. E. and JERDE, E. A. (1987): Diverse eucritic pebbles in the Vaca Muerta mesosiderite. Earth Planet. Sci. Lett., **84**, 1–14.

RUBIN, A. E. and JERDE, E. A. (1988): Compositional differences between basaltic and gabbroic clasts in mesosiderites. Earth Planet. Sci. Lett., **87**, 485–490.

SAIKI, K. and TAKEDA, H. (1990): The chemical map analysis (CMA) study of mesostasis in some Antarcitc eucrites. Papers Presented to the 15th Symposium on Antarctic Meteorites, May 30–June 1, 1990. Tokyo, Natl Inst. Polar Res., 16–17.

STOLPER, E. (1977): Experimental petrology of eucritic meteorites. Geochim. Cosmochim. Acta, **41**, 587–611.

TAYLOR, L. A. and MCCALLISTER, R. H. (1972): An experimental investigation of the significance of zirconium partitioning in lunar ilmenite and ulvospinel. Earth Planet. Sci. Lett., **17**, 105–109.

WARREN, P. H. and JERDE, E. A. (1987): Composition and origin of Nuevo Laredo trend eucrites. Geochim. Cosmochim. Acta, **51**, 713–725.

(Received August 1, 1990; Revised manuscript received October 25, 1990)